RESEARCH ARTICLE

WILEY

HrpB7 from *Xanthomonas campestris* pv. *vesicatoria* is an essential component of the type III secretion system and shares features of HrpO/FliJ/YscO family members

Sabine Drehkopf | Christian Otten | Jens Hausner | Tanja Seifert | Daniela Büttner

Department of Genetics, Institute of Biology, Martin Luther University Halle-Wittenberg, Halle (Saale), Germany

Correspondence
Daniela Büttner, Department of Genetics, Institute of Biology, Martin Luther University Halle-Wittenberg, Weinbergweg 10, 06120 Halle (Saale), Germany.
Email: daniela.buettner@genetik.uni-halle.de

Present address
Jens Hausner, Icon Genetics GmbH, Weinbergweg 22, 06120 Halle (Saale), Germany.

Abstract

The Gram-negative bacterium *Xanthomonas campestris* pv. *vesicatoria* translocates effector proteins via a type III secretion system (T3SS) into eukaryotic cells. The T3SS spans both bacterial membranes and consists of more than 20 proteins, 9 of which are conserved in plant and animal pathogens and constitute the core subunits of the secretion apparatus. T3S in *X. campestris* pv. *vesicatoria* also depends on nonconserved proteins with yet unknown function including HrpB7, which contains predicted N- and C-terminal coiled-coil regions. In the present study, we provide experimental evidence that HrpB7 forms stable oligomeric complexes. Interaction and localisation studies suggest that HrpB7 interacts with inner membrane and predicted cytoplasmic (C) ring components of the T3SS but is dispensable for the assembly of the C ring. Additional interaction partners of HrpB7 include the cytoplasmic adenosinetriphosphatase HrcN and the T3S chaperone HpaB. The interaction of HrpB7 with T3SS components as well as complex formation by HrpB7 depends on the presence of leucine heptad motifs, which are part of the predicted N- and C-terminal coiled-coil structures. Our data suggest that HrpB7 forms multimeric complexes that associate with the T3SS and might serve as a docking site for the general T3S chaperone HpaB.

KEYWORDS
ATPase, C ring, chaperone, coiled coil, effector protein, leucine heptad motifs, plant pathogenic bacterium, type III secretion

1 | INTRODUCTION

The Gram-negative plant pathogenic bacterium *Xanthomonas campestris* pv. *vesicatoria* (*Xcv*; also designated *X. euvesicatoria* [Jones, Lacy, Bouzar, Stall, & Schaad, 2004]) is the causal agent of bacterial spot disease on pepper and tomato plants and one of the model organisms for the analysis of bacterial infection strategies (Büttner & Bonas, 2010). Pathogenicity of *Xcv* depends on the translocation of effector proteins into plant cells where they interfere with essential plant cellular processes and thus promote bacterial proliferation (Büttner, 2016; Büttner & Bonas, 2010; Dean, 2011). Effector protein delivery is mediated by a type III secretion (T3S) system, which is present in many Gram-negative plant and animal pathogenic bacteria and is related to the bacterial flagellum. Both systems are, therefore, referred to as translocation-associated and flagellar T3SS (Abby & Rocha, 2012; Büttner, 2012). The membrane-spanning secretion apparatus of both systems contains at least eight conserved core components, which are known as secretion and cellular translocation (Sct) proteins in animal pathogenic bacteria followed by a letter

corresponding to the nomenclature of T3SS components from *Yersinia* spp. (Hueck, 1998).

Structural studies of isolated T3SSs from animal pathogenic bacteria revealed the presence of ring components in both bacterial membranes (Büttner, 2012; Deng et al., 2017). The outer membrane (OM) ring, also termed secretin, consists of members of the SctC protein family and is connected on the extracellular side to a pilus-like structure known as T3S needle in animal and T3S pilus in plant pathogenic bacteria. T3S needles or pili serve as transport channels for effector proteins to the eukaryotic plasma membrane (Büttner, 2012; Deng et al., 2017). On the periplasmic side, the OM ring is in contact with an inner rod structure and the inner membrane (IM) rings, which are assembled by SctD and SctJ proteins (Büttner, 2012; Deng et al., 2017; Diepold & Wagner, 2014). Embedded in the IM rings is the export apparatus, which presumably forms a transport channel for secreted proteins and consists of members of the SctU, SctV, SctR, SctS, and SctT families (Büttner, 2012; Deng et al., 2017; Lara-Tejero & Galan, 2019). The export apparatus associates with the cytoplasmic adenosinetriphosphatase (ATPase) complex (SctN and SctL), which presumably unfolds T3S substrates and is surrounded by a predicted cytoplasmic ring (C ring) or pod-like structures as was described for several T3SSs from animal pathogenic bacteria. C ring or pod-like structures are assembled by members of the SctQ family and are presumably involved in substrate recognition (Diepold et al., 2015; Hu et al., 2015; Lara-Tejero, 2019; Makino et al., 2016; Morita-Ishihara et al., 2006; Spaeth et al., 2009).

To date, the architecture and mode of action of T3SSs have been intensively studied in animal pathogenic bacteria, whereas much less is known about T3SSs from plant pathogenic bacteria. T3S genes from plant pathogens were designated hypersensitive response and pathogenicity (*hrp*) because they are essential for disease symptoms on susceptible plants and the induction of the effector-triggered immunity in resistant plants (Büttner & He, 2009; Schmidt & Hensel, 2004; Tampakaki et al., 2010). Effector-triggered immunity depends on the recognition of individual effectors in plants with cognate resistance genes and often leads to the induction of the hypersensitive response (HR), a local cell death at the infection site, which restricts bacterial multiplication (Gill et al., 2015). Hrp-T3SSs from plant pathogenic bacteria have been classified into Hrp1- (in *Erwinia* spp. and *Pseudomonas syringae* pathovars) and Hrp2-T3SSs (in *Xanthomonas* spp. and *Ralstonia solanacearum*) according to similarities in the genetic organisation and regulation of *hrp* genes (Alfano & Collmer, 1997; Bogdanove et al., 1996; Troisfontaines & Cornelis, 2005). In *Xcv*, *hrp* genes are activated when the bacteria enter the plant or are cultivated in special minimal media. *hrp* gene expression depends on two regulatory proteins, HrpG and HrpX, which are encoded outside the *hrp* gene cluster (Büttner & Bonas, 2002; Büttner & Bonas, 2010; Wengelnik & Bonas, 1996; Wengelnik et al., 1996). HrpG is an OmpR-type response regulator that perceives an environmental signal via a yet unknown mechanism and activates HrpX, an AraC-type transcriptional regulator (Wengelnik et al., 1996; Wengelnik & Bonas, 1996). HrpX binds to conserved DNA motifs in the promoter regions of most *hrp* operons and activates *hrp* gene expression (Koebnik, et al., 2006; Noël et al, 2001).

The *hrp* gene cluster from *Xcv* contains eight operons with 25 genes including 11 conserved *hrc* (*hrp* conserved), 7 non-conserved *hrp*, and 6 *hpa* (*hrp* associated) genes as well as the effector gene *xopF1* (Büttner & Bonas, 2002). *hrc* genes encode the core components of the T3SS such as the ATPase, the membrane rings, the predicted C ring, and the ATPase complex. The single-letter nomenclature of Hrc proteins refers to the corresponding Sct proteins from animal pathogens (Bogdanove et al., 1996; Büttner & Bonas, 2002). In contrast to Hrc proteins, Hrp proteins are not widely conserved, and homologues are mainly found within one bacterial species. Hrp proteins from *Xcv* and other *Xanthomonas* spp. include the predicted periplasmic inner rod proteins HrpB1 and HrpB2, the pilus protein HrpE, the translocon protein HrpF, and proteins of yet unknown function such as HrpB4, HrpB7, and HrpD6 (Büttner et al., 2002; Hartmann et al., 2012; Hausner et al., 2013; Li et al., 2011; Weber et al., 2005; Weber & Koebnik, 2005). Hrc and Hrp proteins are essential for T3S as structural components, whereas the accessory Hpa (Hrp associated) proteins are often involved in the control of T3S. One example is the T3S chaperone HpaB, which binds to type III effectors and presumably targets them to the T3S ATPase (Büttner et al., 2004; Büttner et al., 2006; Lonjon et al., 2017; Lorenz & Büttner, 2009; Prochaska et al., 2018; Scheibner et al., 2018). HpaB contributes to the translocation of most effector proteins and is, therefore, essential for pathogenicity.

Focus of the present study is the functional characterisation of HrpB7, which is encoded downstream of the ATPase gene *hrcN* by the seventh gene in the *hrpB* operon. HrpB7 is conserved in *Xanthomonas* spp. and shares amino acid sequence identity with HrpD from *R. solanacearum*. In *Xcv*, HrpB7 is the only *hrp* gene product with predicted N- and C-terminal coiled coils and contains features of HrpO/FliJ/YscO family members, which are small α-helical coiled-coil proteins encoded downstream of the T3S-ATPase genes from plant and animal pathogenic bacteria. In the present study, we show that HrpB7 from *Xcv* is required for secretion and translocation of early and late T3S substrates. HrpB7 forms stable protein complexes even in the absence of the T3SS and interacts with the ATPase and the predicted C ring, suggesting that it is a cytoplasmic structural component of the T3SS. The analysis of HrpB7 mutant derivatives by in vitro and in vivo studies revealed that protein function and complex formation depend on the N- and C-terminal leucine heptad motifs, which are part of the predicted coiled-coil structures of HrpB7 and are presumably involved in protein–protein interactions.

2 | RESULTS

2.1 | HrpB7 contains leucine heptad motifs and regularly spaced cysteine residues

HrpB7 from *Xcv* strain 85–10 is a small protein (169 amino acids), encoded downstream of the ATPase gene *hrcN* by the seventh gene
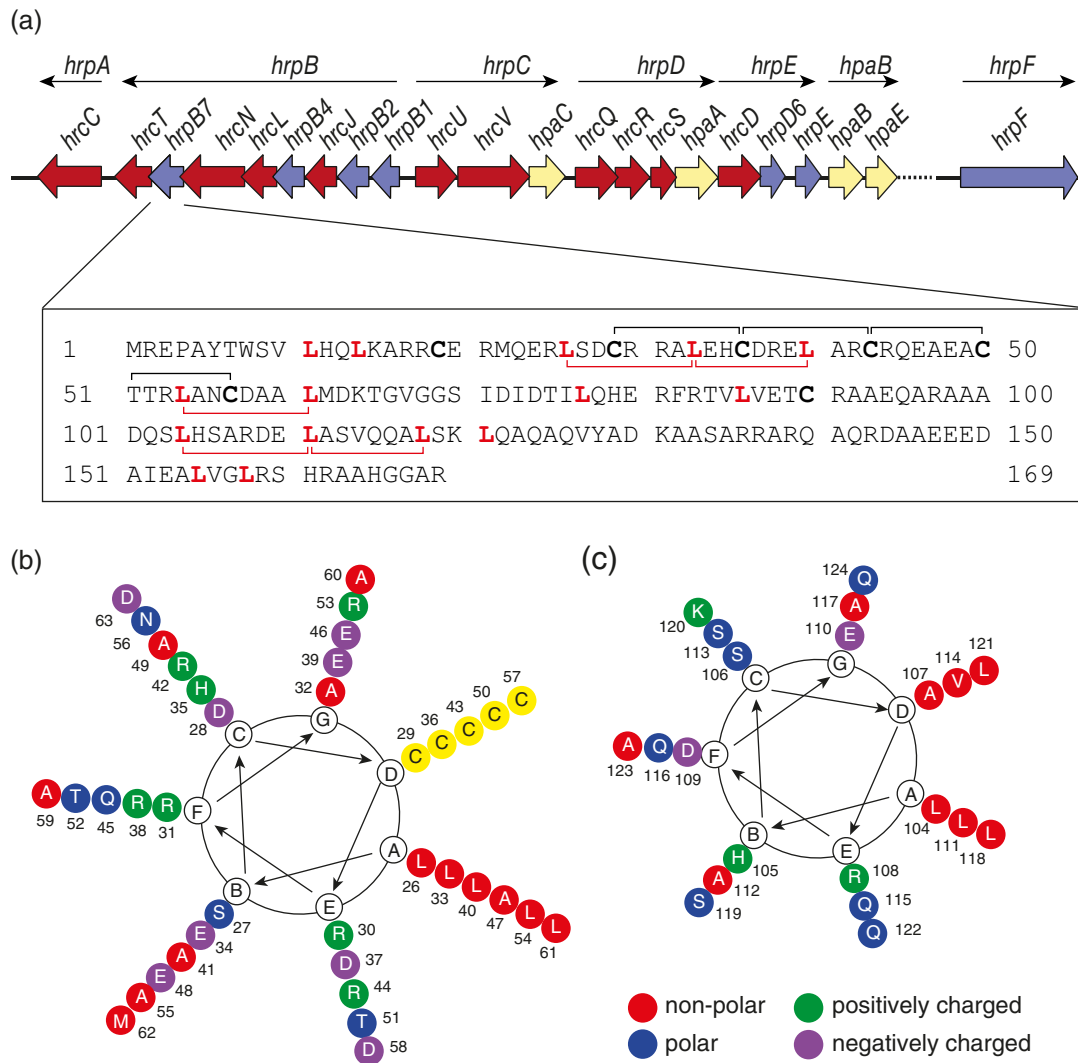
FIGURE 1 HrpB7 contains leucine heptad motifs and regularly spaced cysteine residues. (a) Schematic representation of the *hrp* gene cluster and amino acid sequence of HrpB7 (accession number CAJ22064). *hrc*, *hrp*, and *hpa* genes of the *hrp* gene cluster are represented by red, purple, and yellow arrows, respectively. The direction of transcription of single *hrp* operons is indicated. The *xopF1* operon between *hpaE* and *hrpF*, which encodes the effector protein XopF1 and two putative associated chaperones, is replaced by a dashed line. The amino acid sequence of HrpB7 is given below the *hrp* gene cluster. HrpB7 contains leucine heptad motifs (indicated by red brackets) and five N-terminal regularly spaced cysteine residues, which are shown in bold letters. Numbers refer to amino acid positions. (b) Helical wheel representation of the N-terminal leucine heptad motifs in HrpB7. The letters A–G in the inner circle refer to amino acid positions 1–7 in the heptad motifs (see text), respectively. Amino acids are shown in coloured circles; numbers refer to the amino acid positions. Red circles represent amino acids with nonpolar residues. Blue, green, and purple circles refer to amino acids with polar, positively, and negatively charged amino acids, respectively, as indicated. Cysteine residues are represented by yellow circles. (c) Helical wheel representation of the C-terminal leucine heptad motifs in HrpB7. Amino acids are presented as described in the helical wheel representation of the N-terminal leucine heptad motifs in HrpB7 (b)

of the *hrpB* operon (Figure 1a). The N-terminal region of HrpB7 (amino acids 28–57) contains a motif of five regularly spaced cysteine residues (C-X$_6$)$_5$, each separated from the neighbouring cysteine residue by six amino acids. This motif overlaps with a leucine-heptad motif (L-X$_6$-L-X$_6$-L) consisting of leucine residues at every seventh position (amino acids 26 to 40; Figure 1a,b). Additional leucine heptad motifs are at amino acids 54 to 61 and 104 to 121 (Figure 1a,c). Heptad motifs (also referred to as [abcdefg]$_n$) are often part of alpha-helical coiled-coil structures and form two helical turns (3.5 amino acids per turn) with amino acids at positions "a" and "d" being

generally hydrophobic, for example, leucine, valine, or isoleucine (Lupas & Gruber, 2005; Mason & Arndt, 2004). Given the three-dimensional structure of the helix, residues at positions "a" and "d" are in close proximity to each other at one side of the helix, thus forming a hydrophobic region that stabilises the helical structure and can promote protein dimerisation or oligomerisation via hydrophobic interactions (Mason & Arndt, 2004; Figure 1b,c). In contrast to the "a" and "d" residues, positions "e" and "g" are usually occupied by solvent-exposed polar or charged residues (Mason & Arndt, 2004). Opposite charges at positions "e" and "g" within one helix or in

FIGURE 2 Analysis of an *Xcv hrpB7* deletion mutant. (a) HrpB7 is essential for pathogenicity of *Xcv*. Strains 85–10 (wt), 85* (wt), and corresponding *hrpB7* deletion mutants (Δ*hrpB7*) with or without (−) expression constructs encoding HrpB7 as indicated were infiltrated at a density of 10^8 CFU ml^{-1} into leaves of susceptible ECW and resistant ECW-10R pepper plants. Disease symptoms were photographed 7 days post inoculation (dpi; for derivatives of strain 85*) and 10 dpi (for derivatives of strain 85–10). For the better visualisation of the HR, leaves were destained in ethanol 2 dpi. Dashed lines indicate the inoculated areas. HrpB7 was stably synthesised as is shown in Figure S2. (b) *In planta* growth of the *hrpB7* deletion mutant. *Xcv* wild-type strain 85–10, the *hrpB7* deletion mutant 85–10Δ*hrpB7*, and the ATPase-deficient strain 85–10Δ*hrcN* were infiltrated at a density of 10^4 CFU ml^{-1} into leaves of susceptible pepper plants. Bacterial population densities were determined 0–11 dpi as mean values of three different samples from three different plants. Error bars represent standard deviations. Growth curves were performed three times with comparable results. The results of one representative experiment are shown. (c) Complementation studies with HrpB7 from Xcv and Xcc. Xcv strains 85* (wt) and 85*Δ*hrpB7* (Δ*hrpB7*) without expression construct (−) or containing HrpB7$_{Xcv}$-c-Myc or HrpB7$_{Xcc}$-c-Myc as indicated were infiltrated into leaves of susceptible ECW and resistant ECW-10R pepper plants. Disease symptoms were photographed 8 dpi. Leaves of resistant plants were destained in ethanol 2 dpi. Dashed lines indicate the inoculated areas. (d) Detection of HrpB7$_{Xcv}$-c-Myc and HrpB7$_{Xcc}$-c-Myc. For protein detection, *Xcv* strains as described in complementation studies with HrpB7 (c) were grown in complex medium, and equal amounts of cell extracts were analysed by SDS-PAGE and immunoblotting, using a c-Myc epitope-specific antibody. Monomeric HrpB7 and predicted HrpB7 complexes are indicated by arrows. ECW, Early Cal Wonder

neighbouring helices likely stabilise the coiled coil structure (Mason & Arndt, 2004). In the N-terminal two leucine heptad motifs of HrpB7, these criteria are fit when the leucine residues are located at position "a" and the regularly spaced cysteine residues of the (C-X$_6$)$_5$ motif at position "d" of each repeat (Figure 1b). In the C-terminal leucine heptad motif, position "d" is occupied by the nonpolar amino acids alanine, valine, and leucine (Figure 1c). In agreement with the presence of leucine heptad motifs in

HrpB7, the analysis of the predicted secondary protein structure by Phyre2 (Kelley, et al., 2015) and SWISS-MODEL (Waterhouse et al., 2018) revealed a predominantly alpha-helical conformation of HrpB7 (Figure S1). Furthermore, coiled-coil structures were predicted for regions spanning amino acids 15 to 50 and 88 to 156 of HrpB7 (prediction by programme coiled coil prediction; https://npsa-prabi.ibcp.fr/cgi-bin/npsa_automat.pl?page=npsa_lupas.html).

TABLE 1 Characteristics of HrpB7 derivatives with mutations in leucine and cysteine residues

HrpB7 derivative	Mutations[a]	Epitope[b]	Protein function[c]	Complex formation[d]
HrpB7$_{C3A}$	C43A	None	+	+
		c-Myc	+	+
HrpB7$_{C1-2A}$	C29,36A	None	+	+
		c-Myc	+	+
HrpB7$_{C1-3A}$	C29,36,43A	None	+	+
		c-Myc	+	+
HrpB7$_{C1-5A}$	C29,36,43,50,57A	None	Reduced	Reduced
		c-Myc	−	Reduced
HrpB7$_{C6A}$	C90A	None	+	+
		c-Myc	+	+
HrpB7$_{C1-6A}$	C29,36,43,50,57,90A	None	Reduced	Reduced
		c-Myc	−	Reduced
HrpB7$_{L1S}$	L33,40S	c-Myc	+	+
HrpB7$_{L1G}$	L33,40G	c-Myc	+	+
HrpB7$_{L2S}$	L111,118S	c-Myc	+	Reduced
HrpB7$_{L2G}$	L111,118G	c-Myc	+	Reduced
HrpB7$_{L12S}$	L33,40,111,118S	None	+	−
		c-Myc	+	−
HrpB7$_{L12G}$	L33,40,111,118G	None	Reduced	−
		c-Myc	−	−

[a]Numbers refer to amino acid positions in HrpB7.
[b]Proteins were analysed as untagged or C-terminally c-Myc epitope-tagged derivatives.
[c]Protein function was analysed in strain 85∗ΔhrpB7 by infection experiments. + indicates complementation of the hrpB7 mutant phenotype with respect to disease symptoms and HR induction in susceptible and resistant pepper plants, respectively; − indicates no complementation of the hrpB7 mutant phenotype; reduced indicates partial complementation of the hrpB7 mutant phenotype.
[d]Complex formation was analysed by immunoblotting of bacterial protein extracts. + indicates that HrpB7 complexes were detectable; − indicates that no complex formation was detectable; reduced indicates reduced complex formation.

2.2 | Complementation studies with a nonpolar hrpB7 deletion mutant

Previous transposon mutagenesis approaches showed that a disruption of the hrpB7 gene results in a loss of pathogenicity of Xcv (Bonas et al., 1991; Fenselau & Bonas, 1995). To further assess the contribution of HrpB7 to pathogenicity, we deleted codons 7 to 164 of hrpB7 from the genome of Xcv strain 85–10 and analysed pathogenicity and in planta growth of the resulting mutant strain. In contrast to the wild type, strain 85–10ΔhrpB7 failed to induce water-soaked lesions in susceptible Early Cal Wonder (ECW) pepper plants and was severely affected in in planta growth (Figure 2a,b). Furthermore, strain 85–10ΔhrpB7 did not induce the HR on ECW-10R pepper plants, which contain the Bs1 resistance gene for recognition of the effector protein AvrBs1 (Minsavage et al., 1990; Figure 2a). We observed similar phenotypes with derivatives of strain 85∗ (85-10hrpG∗), which contains a constitutively active version of the regulator HrpG and elicits faster plant reactions than the wild-type strain (Figure 2a; Rossier et al., 1999; Wengelnik et al., 1999). The hrpB7 mutant phenotype was complemented by ectopic expression of hrpB7 under control

of the lac promoter, suggesting that it was specifically caused by the absence of hrpB7 and not by a polar effect of the deletion on the expression of the downstream hrcT gene (Figure 2a). This is an important control because hrpB7 from Xanthomonas oryzae pv. oryzicola was reported to contain a promoter for the downstream hrcT gene, which encodes an essential component of the export apparatus (Liu et al., 2014).

We also performed complementation studies with C-terminally c-Myc epitope-tagged derivatives of HrpB7 from Xcv and X. campestris pv. campestris (Xcc; HrpB7$_{Xcc}$), which share 70% amino acid identity (77% sequence similarity) and show sequence variations in some of the N-terminal leucine and cysteine residues (Figure S1). Both proteins restored pathogenicity in strain 85∗ΔhrpB7, suggesting that they were functional (Figure 2c). In contrast to HrpB7$_{Xcv}$-c-Myc, HrpB7$_{Xcc}$-c-Myc also fully complemented the phenotype of strain 85–10ΔhrpB7 with respect to disease symptoms and the HR (Figure S2). Given that the ectopic expression of hrpB7$_{Xcv}$-c-myc in strain 85–10 suppressed the elicitation of plant reactions, we assume that enhanced levels of HrpB7$_{Xcv}$-c-Myc but not of HrpB7$_{Xcc}$-c-Myc interfere with pathogenicity in strain 85–10 (Figure S2). Immunoblot analysis showed that all
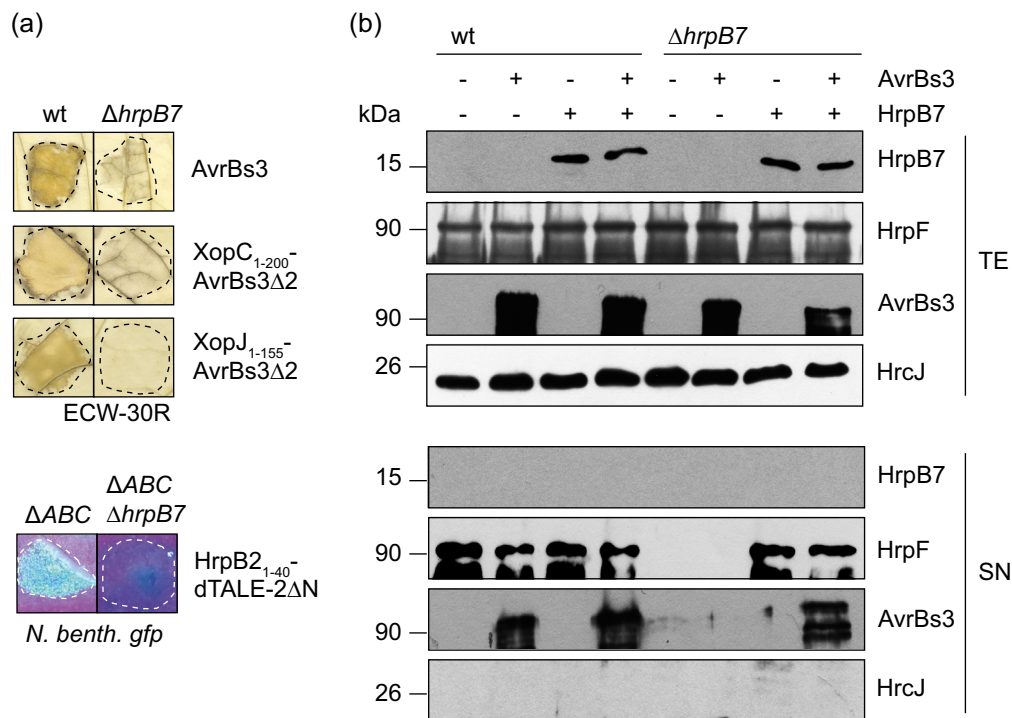
FIGURE 3 HrpB7 is essential for T3S-dependent protein delivery. (A) HrpB7 is essential for translocation of early and late T3S substrates. Strains 85* and 85*ΔhrpB7 (ΔhrpB7) with expression constructs encoding AvrBs3 or the AvrBs3Δ2 fusion proteins XopC$_{1-200}$-AvrBs3Δ2 and XopJ$_{1-155}$-AvrBs3Δ2 as indicated were infiltrated at a density of 4×10^8 CFU ml^{-1} into leaves of AvrBs3-responsive Early Cal Wonder-30R pepper plants. For the better visualisation of the hypersentitive response, leaves were bleached in ethanol 2 days post inoculation. For the analysis of the early T3S substrate HrpB2, strains 85*ΔhpaABC (ΔABC) and 85*ΔhpaABCΔhrpB7 (ΔABCΔhrpB7) containing HrpB2$_{1-40}$-dTALE-2ΔN were inoculated at a density of 4×10^8 CFU ml^{-1} into leaves of gfp-transgenic Nicotiana benthamiana plants. Leaves were photographed 7 days post inoculation. Dashed lines indicate the inoculated areas. AvrBs3 and fusion proteins were stably synthesised in all strains (data not shown). (b) HrpB7 is essential for T3S and is itself not secreted by the T3SS. Strains 85* (wt) and 85*ΔhrpB7 (ΔhrpB7) with (+) or without (−) expression constructs encoding HrpB7 or AvrBs3 as indicated were incubated in secretion medium. TE and culture SN were analysed by immunoblotting using antibodies specific for HrpB7, the translocon protein HrpF, the effector AvrBs3, and the inner membrane ring protein HrcJ, respectively. The upper protein detected by the AvrBs3-specific antibody corresponds to full-length AvrBs3, lower signals likely result from the detection of degradation products. TE, total cell extracts; SN, supernatants

HrpB7 derivatives were stably synthesised (Figures 2d and S2). In addition to the monomeric HrpB7 and HrpB7-c-Myc proteins at the predicted sizes of 18 and 23 kDa, respectively, HrpB7-specific signals were detected at higher molecular sizes, suggesting the presence of HrpB7-containing protein complexes, which were not dissolved by SDS-PAGE (Figures 2d and S2; see below).

2.3 | HrpB7 is essential for T3S and effector translocation

In addition to infection studies, we investigated the contribution of HrpB7 to the T3S-dependent delivery of the transcription activator-like (TAL) effector protein AvrBs3, which activates expression of the resistance gene Bs3 in AvrBs3-responsive ECW-30R pepper plants (Boch et al., 2009; Römer et al., 2009). Furthermore, we used the N-terminal deletion derivative AvrBs3Δ2, which lacks a native export signal, as a reporter to monitor the translocation of the effector proteins XopC and XopJ. When AvrBs3 and AvrBs3Δ2 fusion proteins were analysed in strain 85*, which naturally lacks the avrBs3 gene,

they induced the AvrBs3-specific HR in ECW-30R pepper plants as expected (Minsavage et al., 1990; Noël et al., 2003; Römer et al., 2009; Szurek et al., 2002). No HR induction was observed with strain 85*ΔhrpB7, suggesting that translocation depends on HrpB7 (Figure 3a). We also analysed the influence of HrpB7 on the export of the early T3S substrate HrpB2, which is translocated in the absence of the control proteins HpaA, HpaB, and HpaC (Lorenz & Büttner, 2011; Rossier et al., 2000; Scheibner et al., 2016; Weber et al., 2005). An N-terminal deletion derivative of the designer TAL effector dTALE-2 was used as a reporter to monitor translocation of HrpB2 in transgenic Nicotiana benthamiana plants, which contained the green fluorescent protein (gfp) gene on a viral construct under control of a dTALE-2-responsive promoter (Weber et al., 2011; Werner, Breus, Symonenko, Marillonnet, & Gleba, 2011). The fusion protein HrpB2$_{1-40}$-dTALE-2ΔN was efficiently translocated by strain 85*ΔhpaABC, thus leading to GFP fluorescence in gfp-transgenic N. benthamiana plants as expected (Scheibner et al., 2016; Figure 3a). Additional deletion of hrpB7 in strain 85*ΔhpaABC, however, abolished GFP fluorescence, suggesting an essential role of HrpB7 for the translocation of both early and late T3S substrates (Figure 3a).
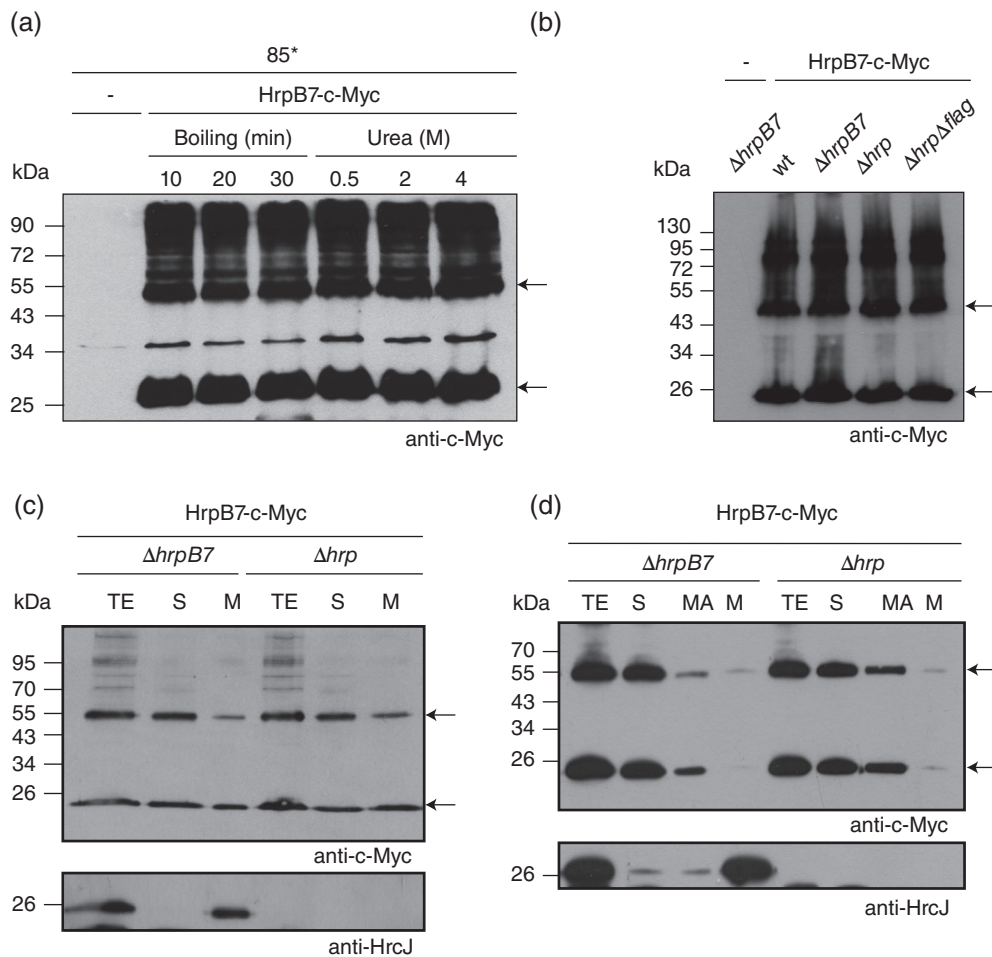
FIGURE 4 HrpB7 forms complexes and associates with the bacterial membranes. (a) HrpB7 complexes are not dissolved upon prolonged boiling or addition of urea. Strain 85* without expression construct (−) or ectopically expressing *hrpB7-c-myc* was grown in complex medium, and equal amounts of cell extracts (adjusted according to the optical density of the cultures) were analysed by immunoblotting using a c-Myc epitope-specific antibody. Monomeric HrpB7 and predicted HrpB7 dimer are indicated by arrows. Protein extracts were treated either by prolonged boiling (10, 20, and 30 min instead of 5 min as indicated) or by the addition of urea at final concentrations of 0.5, 2, or 4 M. The experiment was performed twice with similar results. (b) HrpB7-c-Myc forms complexes independently of the T3SS. Strains 85* (wt), 85*Δ*hrpB7* (Δ*hrpB7*), 85*Δ*hrp* (Δ*hrp*), and 85*Δ*hrpΔflag* (Δ*hrpΔflag*) without expression construct (−) or containing HrpB7-c-Myc as indicated were grown in complex medium, and equal amounts of cell extracts were analysed by immunoblotting using a c-Myc epitope-specific antibody. Monomeric HrpB7 and predicted HrpB7 dimers are indicated by arrows. (c) HrpB7 localises to the bacterial cytoplasm, and the membranes independently of the T3SS. Strains 85*Δ*hrpB7* (Δ*hrpB7*) and 85*Δ*hrp* (Δ*hrp*) containing HrpB7-c-Myc were grown in minimal medium under T3S-permissive conditions, and S and M fractions were separated by ultracentrifugation. TE, M, and S were analysed by immunoblotting using antibodies specific for the c-Myc epitope and the inner membrane ring protein HrcJ, respectively. Monomeric HrpB7 and predicted HrpB7 complexes are indicated by arrows. (d) HrpB7 associates with the bacterial membranes. Strains 85*Δ*hrpB7* (Δ*hrpB7*) and 85*Δ*hrp* (Δ*hrp*) containing HrpB7-c-Myc were cultivated as described in panel (c), and soluble and membrane fractions were separated by ultracentrifugation. Membrane fractions were subsequently incubated in the presence of 5-M urea and MA proteins were separated from integral M proteins by ultracentrifugation. TE, S, MA, and M fractions were analysed by immunoblotting as described in panel (c). M, membrane; MA, membrane-associated proteins; S, soluble; TE, total cell extracts

To study the influence of HrpB7 on in vitro T3S, bacteria were incubated in secretion medium, and total cell extracts and culture supernatants were analysed by immunoblotting. The translocon protein HrpF and the effector protein AvrBs3 (ectopically expressed from a plasmid) were detected in the culture supernatant of strain 85* but not of strain 85*Δ*hrpB7* (Figure 3b). In contrast, the predicted IM ring protein HrcJ, which was analysed as lysis control, was only detected in total cell extracts as expexted (Figure 3b). We also investigated a possible secretion of HrpB7 in strains 85* and 85*Δ*hrpB7* containing *hrpB7* or *hrpB7-c-myc* expression constructs. HrpB7 and HrpB7-c-

Myc were detected in total cell extracts but not in the culture supernatants, suggesting that HrpB7 is not secreted under the conditions tested (Figures 3b and S3).

2.4 | HrpB7 forms stable protein complexes and localises to bacterial membranes

As mentioned above, HrpB7 presumably forms complexes corresponding to mono- or heterooligomers in the presence of SDS and

(a)

ECW

(b)
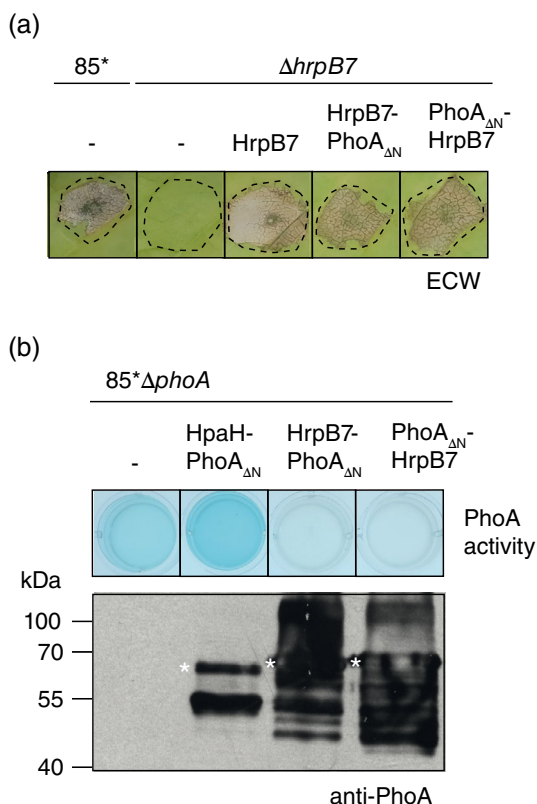
FIGURE 5 Localisation studies with HrpB7-PhoA$_{\Delta2-120}$ fusions. (a) HrpB7-PhoA$_{\Delta2-120}$ fusions complement the *hrpB7* mutant phenotype. Strains 85* and 85*Δ*hrpB7* (Δ*hrpB7*) with or without (−) expression constructs encoding HrpB7, HrpB7-PhoA$_{\Delta2-120}$ (PhoA$_{\Delta N}$), or PhoA$_{\Delta N}$-HrpB7 as indicated were infiltrated at a density of 10^8 CFU ml^{-1} into leaves of susceptible ECW plants. Disease symptoms were photographed 8 days post inoculation. Dashed lines indicate the inoculated areas. (b) Analysis of PhoA activities of HrpB7-PhoA$_{\Delta2-120}$ fusions. Strains 85* and 85*Δ*hrpB7* (Δ*hrpB7*) with or without (−) expression constructs encoding PhoA$_{\Delta2-120}$ (PhoA$_{\Delta N}$) fusion proteins as indicated were incubated in secretion medium, and phosphatase activity was analysed as described in Section 4. Proteins were detected by immunoblotting as described in panel (a). PhoA$_{\Delta2-120}$ fusions are indicated by asterisks. The fusion between the periplasmic predicted lytic transglycosylase HpaH and PhoA$_{\Delta2-120}$ was analysed as positive control (Hausner et al., 2017). ECW, Early Cal Wonder

β-mercaptoethanol (Figure 2d). Complexes were very stable and were also detected upon prolonged boiling or addition of urea (Figure 4a). Furthermore, complex formation was unaffected when *hrpB7* was expressed in *Xcv* strains 85*Δ*hrp* and 85*Δ*hrp*Δ*flag*, which lack the complete *hrp* gene cluster and additionally essential parts of the flagellar T3S gene cluster, respectively (Figure 4b). We conclude that HrpB7 multimerises independently of the T3SS.

Next, we analysed whether HrpB7 associates with the bacterial membranes. For this, strains 85*Δ*hrpB7* and 85*Δ*hrp* containing HrpB7-c-Myc were grown in minimal medium under T3S-permissive conditions (pH 5.3), and soluble and membrane fractions were separated by ultracentrifugation. HrpB7-c-Myc was detected in the soluble and the membrane fractions of both strains, suggesting that the

association of HrpB7 with the bacterial membranes was independent of the T3SS (Figure 4c). As control, blots were reprobed with an antibody directed against the IM ring component HrcJ, which was mainly detected in the membrane fraction of strain 85*Δ*hrpB7* as expected (Figure 4c). Similar results were obtained when bacteria were incubated under T3S nonpermissive conditions (minimal medium, pH 7.0; Figure S4). As HrpB7 lacks predicted transmembrane domains, it is likely not an integral membrane protein. To prove this hypothesis, we incubated the membrane fractions in the presence of 5-M urea and separated integral membrane proteins from membrane-associated proteins by ultracentrifugation. HrpB7 was predominantly detected in the membrane-associated fraction, which is in agreement with the hypothesis that HrpB7 does not insert into the IM or OM (Figure 4d). Similar results were obtained when bacteria were incubated under T3S nonpermissive conditions (Figure S4).

To further investigate the subcellular localisation of HrpB7, we generated N- and C-terminal fusions of HrpB7 to an N-terminal deletion derivative of the alkaline phosphatase PhoA (PhoA$_{\Delta2-120}$) from *Escherichia coli*, which is active when located in the periplasm and used as a reporter to analyse protein topology (Berger et al., 2010; Manoil & Beckwith, 1986). HrpB7-PhoA$_{\Delta2-120}$ and PhoA$_{\Delta2-120}$-HrpB7 both complemented the *hrpB7* mutant phenotype, suggesting that the PhoA$_{\Delta2-120}$ fusion partner did not interfere with HrpB7 function (Figure 5a). When analysed in *Xcv* strain 85*Δ*phoA*, which lacks the native *phoA* gene (Hausner et al., 2017), no PhoA activity of both fusions was detectable, suggesting that the N- and C-termini of HrpB7 are not located in the periplasm (Figure 5b). Given the absence of predicted transmembrane domains in HrpB7, we conclude that HrpB7 localises to the cytoplasmic side of the IM.

2.5 | Cysteine and leucine residues in HrpB7 contribute to protein function and complex formation

To analyse the contribution of single amino acids in HrpB7$_{Xcv}$ to protein function, we exchanged one or several cysteine residues in the N-terminal (C-X$_6$)$_5$ motif against alanine and also introduced mutations leading to the substitution of leucine residues at positions 33 and 40 and/or 111 and 118 by serine or glycine (Table 1). The resulting HrpB7 derivatives were analysed as C-terminally c-Myc epitope-tagged derivatives for their ability to complement the *hrpB7* mutant phenotype. Exchange of the first three cysteine residues of the (C-X$_6$)$_5$ motif or the central cysteine residue at position 90 did not significantly affect HrpB7 function, whereas HrpB7 derivatives with mutations in all five cysteine residues of the (C-X$_6$)$_5$ motif did not complement the *hrpB7* mutant phenotype (Figure 6a; Table 1). Immunoblot analyses of bacterial protein extracts showed that all HrpB7 derivatives were stably synthesised and that formation of HrpB7-specific complexes was significantly reduced or not detectable for HrpB7$_{C1-5A}$-c-Myc and HrpB7$_{C1-6A}$-c-Myc, which was additionally mutated in C90 (Figure 6c; Table 1). When HrpB7 derivatives were analysed as untagged proteins, HrpB7$_{C1-5A}$ and HrpB7$_{C1-6A}$ partially complemented the phenotype of strain

85*ΔhrpB7, suggesting that protein function was not completely abolished (Figure S5; Table 1).

HrpB7 derivatives with mutations in N- or C-terminal leucine heptad motifs (L1S, L1G, L2S, and L2G) complemented the phenotypes of strains 85–10ΔhrpB7 and 85*ΔhrpB7 when analysed as C-terminally c-Myc epitope-tagged (Figure 6b) or untagged proteins (data not shown; Table 1). Substitutions of leucine residues in both heptad motifs by serine had no significant effect (Figures 6b and S6).

In contrast, HrpB7 derivatives in which the leucine residues in both heptad motifs were exchanged against glycine (HrpB7$_{L12G}$) only partially complemented the hrpB7 mutant phenotype when analysed as untagged proteins (Figure S6). No complementation was observed when HrpB7$_{L12G}$ was analysed as C-terminally c-Myc epitope-tagged derivative (Figure 6b; Table 1). This is presumably caused by a negative effect of the c-Myc epitope on protein function (see also Figure S2). Immunoblot analysis showed that complex formation was
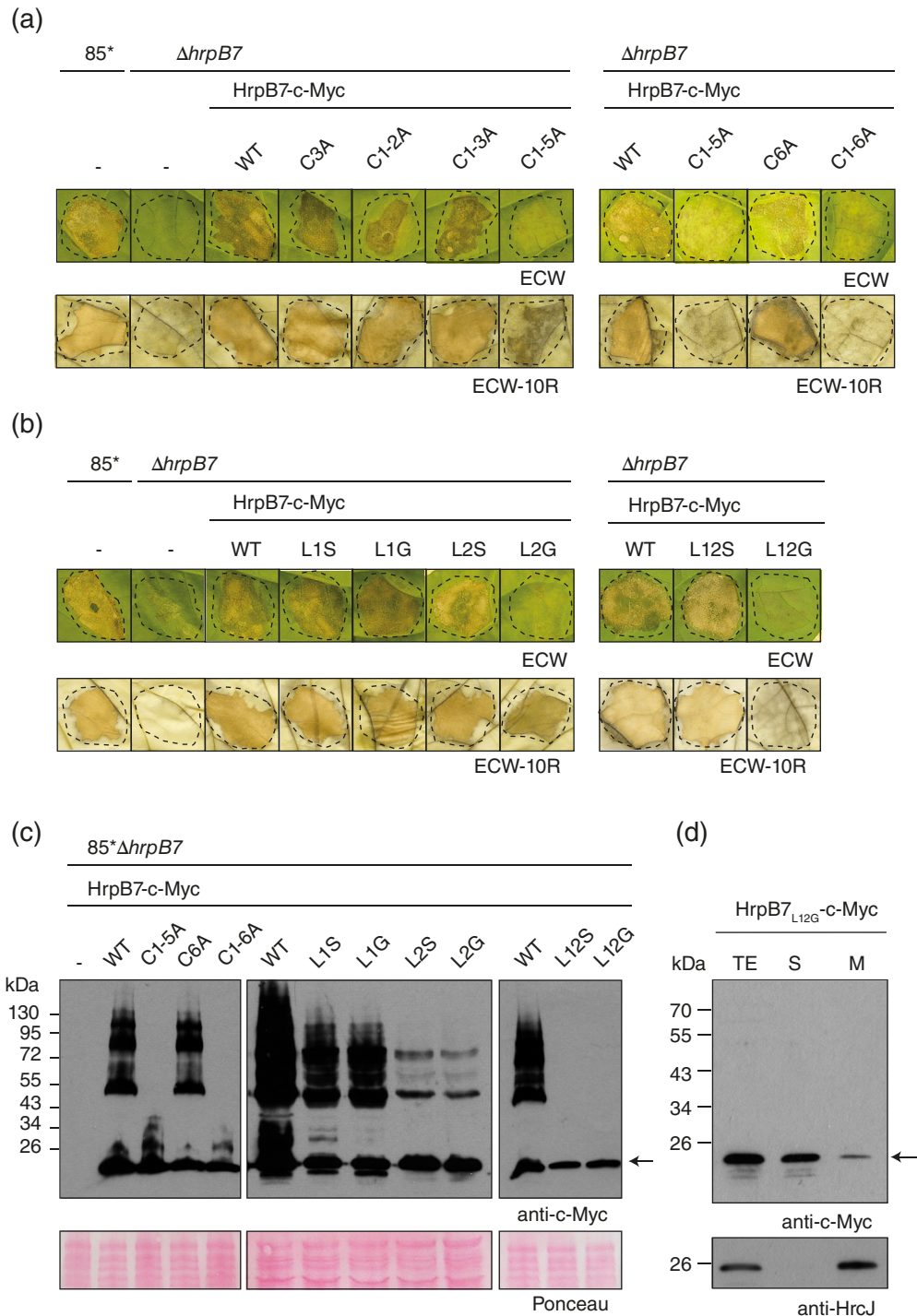
FIGURE 6   Legend on next page.

severely reduced for HrpB7 derivatives carrying substitutions in both leucine heptad motifs, whereas mutations in one motif did not or only slightly interfere with complex formation (Figure 6c). We conclude that both leucine heptad motifs as well as the N-terminal $(C-X_6)_5$ motif of HrpB7 are required for complex formation and contribute to protein function.

We also investigated whether the leucine heptad motifs contribute to the localisation of HrpB7. Fractionation studies with HrpB7$_{L12G}$-c-Myc in strain 85*$\Delta hrpB7$ grown under T3S-permissive conditions revealed that HrpB7$_{L12G}$-c-Myc was predominantly detected in the soluble fraction (Figure 6d). This is in contrast to HrpB7-c-Myc, which was equally distributed in the soluble and membrane fraction (see above; Figure 4d) and suggests that the leucine heptad motifs promote the association of HrpB7 with the bacterial membranes.

2.6 | HrpB7 interacts with components of the T3SS

Next, we analysed whether HrpB7 interacts with components of the T3SS and performed in vitro glutathione S-transferase (GST) pull-down assays. GST and GST-HrpB7 were immobilised on glutathione sepharose and incubated with bacterial lysates containing C-terminally c-Myc epitope-tagged derivatives of potential interaction partners. When eluted proteins were analysed by immunoblotting, the ATPase HrcN, the IM ring protein HrcD, and the predicted C ring protein HrcQ were detected in the eluate of GST-HrpB7 but not of GST, suggesting that they interact with HrpB7 (Figure 7a,b). Similar results were obtained for a C-terminally c-Myc epitope-tagged derivative of the T3S chaperone HpaB (Figure 7a,b). We also investigated a possible contribution of the leucine heptad motifs of HrpB7 to protein–protein interactions. The results of GST pull-down assays suggest that the leucine heptad motifs contribute to the interaction of HrpB7 with HrcQ, HrcD, and HpaB (Figure 7b). This is in agreement with the predicted role of coiled-coil motifs in protein–protein interactions and

supports the hypothesis that coiled-coil motifs contribute to HrpB7 function.

2.7 | HrpB7 is dispensable for the formation of the predicted C ring

Given the potential interaction of HrpB7 with HrcQ, we investigated whether HrpB7 is required for the assembly of the predicted C ring. For this, a fusion protein between HrcQ and the superfolder green fluorescent protein (sfGFP) was analysed in Xcv using a modular T3S gene cluster as described previously (Hausner et al., 2019). As expected, HrcQ-sfGFP formed fluorescent foci, which are indicative of the assembly of the T3SS as was previously described for fluorescent reporter fusions containing T3SS components from animal pathogenic bacteria (Diepold et al., 2010; Diepold et al., 2011; Hausner et al., 2019; Li & Sourjik, 2011; Morimoto et al., 2014; Zhang et al., 2017; Figure 7c,d). Foci formation was dependent on the presence of the T3SS and was not detected in the absence of the hrpA to hpaB operons (Hausner et al., 2019; Figure 7c,d). In the absence of HrpB7, foci formation by HrcQ-sfGFP was only slightly reduced, suggesting that HrpB7 is not essential for the assembly of the predicted C ring (Figure 7c,d).

3 | DISCUSSION

In this study, we identified HrpB7 as a novel complex-forming component of the T3SS from Xcv. Previous transposon mutagenesis approaches already indicated an essential pathogenicity function of HrpB7 (Bonas et al., 1991; Fenselau & Bonas, 1995). This was confirmed in the present study by the analysis of a hrpB7 deletion mutant and complementation studies (Figure 2). The finding that the phenotype of the Xcv hrpB7 mutant can be complemented by HrpB7 from Xcc points to a conserved function of HrpB7 proteins in

FIGURE 6 The N-terminal $(C-X_6)_5$ motif and the leucine heptad motifs contribute to HrpB7 function and complex formation. (a) Strains 85* and 85*$\Delta hrpB7$ ($\Delta hrpB7$) without expression construct (−) or containing expression constructs encoding HrpB7-c-Myc or derivatives thereof with mutations in the $(C-X_6)_5$ motif and/or the central cysteine residue (C6A) as indicated were infiltrated at densities of 4×10^8 CFU ml^{-1} into leaves of susceptible ECW and resistant ECW-10R pepper plants. Disease symptoms were photographed 7 days post inoculation, and leaves of resistant plants were destained in ethanol 2 days post inoculation. Dashed lines indicate the inoculated areas. (b) Strains 85* and 85*$\Delta hrpB7$ ($\Delta hrpB7$) without expression construct (−) or containing expression constructs encoding HrpB7-c-Myc or derivatives thereof with mutations in the N- and C-terminal leucine heptad motifs as indicated were infiltrated into leaves of susceptible ECW and resistant ECW-10R pepper plants. Strains shown on the left panel were infiltrated at densities of 10^8 CFU ml^{-1}, and strains depicted in the right panel at densities of 4×10^8 CFU ml^{-1}. Plant reactions were documented as described in panel (a). L1S, HrpB7$_{L33,40S}$; L1G, HrpB7$_{L33,40G}$; L2S, HrpB7$_{L111,118S}$; L2G, HrpB7$_{L111,118G}$; L12S, HrpB7$_{L33,40,111,118S}$; L12G, HrpB7$_{L33,40,111,118G}$. (c) Leucine heptad motifs and cysteine residues contribute to complex formation. For protein analyses, strain 85*$\Delta hrpB7$ containing HrpB7-c-Myc or derivatives thereof as indicated was grown over night in complex nutrient yeast extract glycerol medium and equal amounts of cell extracts (adjusted according to the optical density) were analysed by immunoblotting, using a HrpB7-specific antibody. Monomeric HrpB7 is indicated by an arrow. Immunoblot analyses of HrpB7$_{C3A}$-c-Myc, HrpB7$_{C1-2A}$-c-Myc, HrpB7$_{C1-3A}$-c-Myc, and of untagged HrpB7 derivatives are shown in Figures S5 and S6. (d) The leucine heptad motif promotes membrane association of HrpB7. Strain 85*$\Delta hrpB7$ containing HrpB7$_{L12G}$-c-Myc was grown in minimal medium under T3S-permissive conditions, and S and M fractions were separated by ultracentrifugation. TE, M, and S fractions were analysed by immunoblotting using antibodies specific for the c-Myc epitope and the inner membrane ring protein HrcJ, respectively. Monomeric HrpB7 is indicated by an arrow. ECW, Early Cal Wonder; M, membrane; S, soluble; TE, total cell extracts
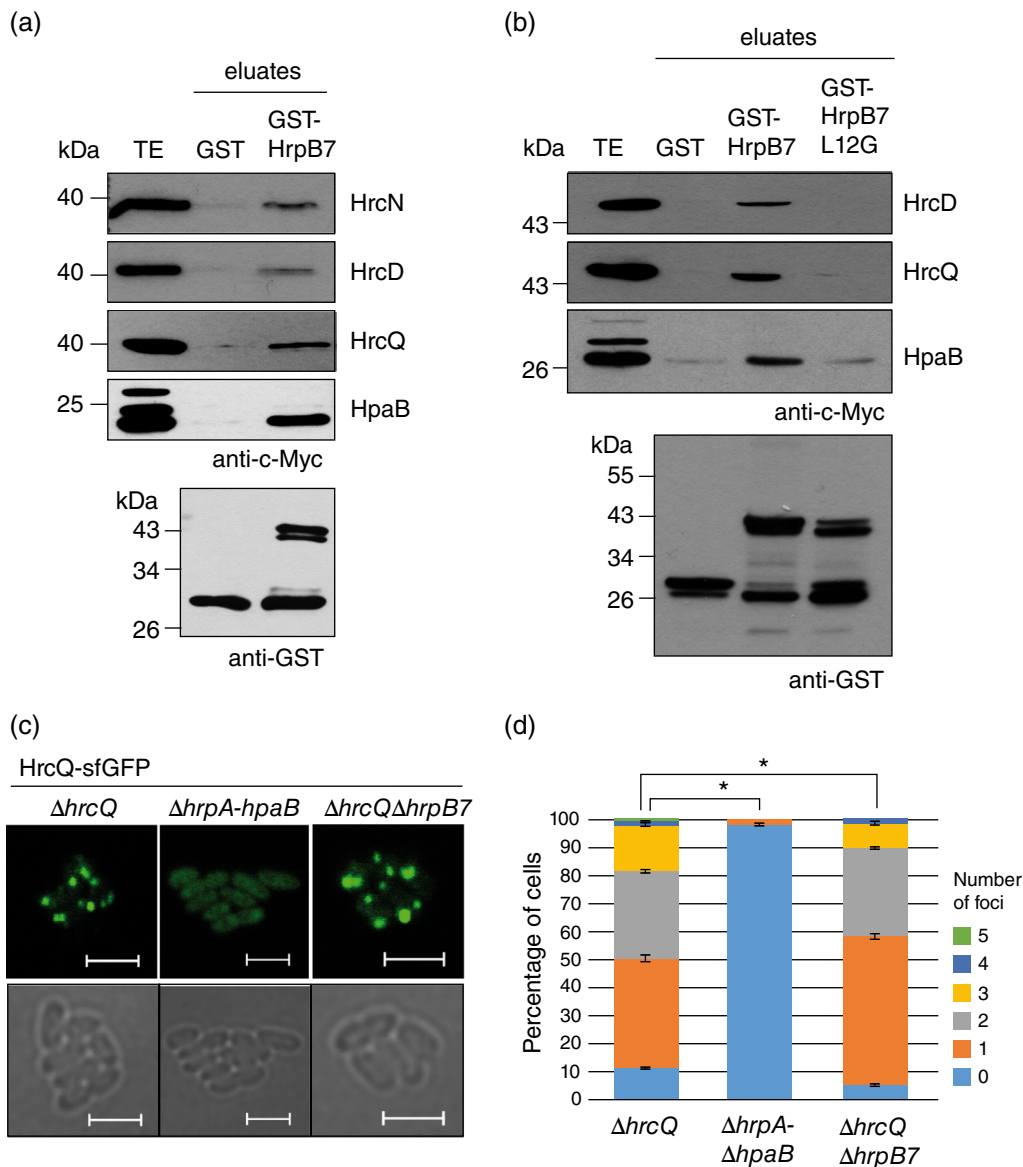
FIGURE 7 HrpB7 interacts with T3S-associated proteins and is dispensable for cytoplasmic ring formation. (a) In vitro interaction studies with HrpB7. GST and GST-HrpB7 were immobilised on glutathione sepharose and incubated with bacterial lysates containing C-terminally c-Myc epitope-tagged derivatives of the ATPase HrcN, the inner membrane ring protein HrcD, the predicted cytoplasmic ring protein HrcQ, and the T3S chaperone HpaB. TE and eluates were analysed by immunoblotting using GST- and c-Myc epitope-specific antibodies as indicated. One representative blot for the detection of GST and GST-HrpB7 is shown. Experiments were performed at least three times with similar results. (b) The leucine heptad motifs of HrpB7 contribute to the interaction with HrcD, HrcQ, and HpaB. GST, GST-HrpB7, and GST-HrpB7$_{L12G}$ were immobilised on glutathione sepharose and incubated with bacterial lysates containing C-terminally c-Myc epitope-tagged derivatives of HrcD, HrcQ, and HpaB. TE and eluates were analysed as described in panel (a). L12G, HrpB7$_{L33,40,111,118G}$. (c) HrpB7 is dispensable for foci formation by HrcQ-sfGFP. Fluorescent foci were analysed in strain 85*Δ*hrp*_fs*HAGX* carrying modular level P *hrp-HAGX* expression constructs containing *hrcQ-sfgfp* and deletions in *hrcQ* (Δ*hrcQ*), in the *hrpA* to *hpaB* operons (Δ*hrpA-hpaB*), as well as in *hrcQ* and *hrpB7* (Δ*hrcQ*Δ*hrpB7*) as indicated. Bacteria were grown in secretion medium, and foci formation was analysed by fluorescence microscopy. The experiment was performed three times with similar results. One representative image for each strain from one experiment is shown. The size bar corresponds to 2 μm. (d) Statistic analysis of HrcQ-sfGFP foci formation. Fluorescent foci were counted in approximately 300 cells per strain in three different transconjugants, and the mean values and standard deviations are shown as percentage of bacterial cells. Asterisks indicate a significant difference between the Δ*hrpA-hpaB* and the *hrcQ* single-deletion mutant strain or the Δ*hrcQ*Δ*hrpB7* and the *hrcQ* single-deletion mutant strain as indicated by brackets with a *p* value < .05 based on the results of a χ^2 test. ECW, Early Cal Wonder; GST, glutathione S-transferase; TE, total cell extracts

Xanthomonas spp. (Figure 2). Notably, however, HrpB7 is not widely conserved in Hrp2-T3SSs and shares only 30% amino acid sequence identity (from amino acids 62–165) with HrpD from *R. solanacearum*, which is also encoded by the seventh gene of the *hrpB* operon. In contrast to HrpB7 from *Xcv*, HrpD contributes to but is not essential for pathogenicity of *R. solanacearum* (Van Gijsegem, et al., 2002). The homology of HrpB7 with HrpD is restricted to the central and C-terminal region of HrpB7 including the C-terminal leucine heptad

motifs, which are part of the predicted coiled-coil structures. HrpB7 is the only *hrp* gene product from *Xcv* with predicted N- and C-terminal coiled coils. This protein motif usually consists of two or more α helices winding around each other and is often involved in protein–protein interactions (Delahay & Frankel, 2002; Woolfson, et al., 2012). In agreement with the presence of predicted coiled coils in HrpB7, our in vitro pull-down assays suggest that HrpB7 interacts with T3SS components including the ATPase HrcN, the predicted C ring protein HrcQ, and the IM ring component HrcD (Figure 7). Furthermore, HrpB7 forms stable complexes, probably corresponding to dimers and homo- or heterooligomers, suggesting that it is part of an oligomeric substructure of the T3SS (Figure 4). Mutations in both N- and C-terminal leucine heptad motifs severely reduced complex formation, thus confirming the predicted contribution of the putative coiled-coil structures to the protein–protein interactions (Figure 6). Given that HrpB7 lacks predicted transmembrane helices and is not secreted and presumably does not localise to the bacterial periplasm, we assume that it associates on the cytoplasmic side with the ATPase complex and the ring structures of the T3SS (Figures 4 and 5).

Notably, complex formation and interaction with the ATPase complex, the C ring and components of the export apparatus were previously reported for T3SS-associated proteins from plant and animal pathogens, which are encoded downstream of the T3S-ATPase genes similarly to HrpB7 (Cherradi et al., 2014; Evans et al., 2006; Fraser et al., 2003; Gazi et al., 2008; Romo-Castillo et al., 2014). Despite a lack of general sequence conservation, these proteins contain predicted coiled coils and are referred to as HrpO/FliJ/YscO protein family (Gazi et al., 2008; Gazi et al., 2009). In addition to HrpB7, the only other characterised member of this protein family from plant pathogenic bacteria is HrpO from *P. syringae*. HrpO was described as α helical with characteristics of intrinsically disordered proteins and self-associates as was also observed for HrpB7. Furthermore, HrpO interacts with the predicted regulator of the T3S-ATPase, HrpE (Gazi et al., 2008; Uversky, 2013). An interaction with the ATPase complex was also reported for the HrpO/FliJ/YscO family members FliJ from the flagellar T3SS, Spa13 from *Shigella flexneri*, and EscO (formerly known as Orf15 or EscA) from enteropathogenic *E. coli* (Cherradi et al., 2014; Evans et al., 2006; Romo-Castillo et al., 2014). EscO stimulates the activity of the ATPase EscN in vitro in the absence of the negative regulator EscL and enhances EscN hexamerisation (Majewski et al., 2019; Romo-Castillo et al., 2014). A similar positive effect on the ATPase activity was described for FliJ, which promotes hexamerisation of the ATPase FliI of the flagellar T3SS (Ibuki et al., 2011). FliJ and EscO share structural similarity with the α-helical coiled-coil region of the F_0F_1 ATPase γ subunit, which is part of the central stalk of the ATPase (Ibuki et al., 2011; Majewski et al., 2019). It was, therefore, suggested that HrpO/FliJ/YscO family members associate with the ATPase complex and are involved in the regulation of the ATPase activity. In agreement with this hypothesis, the crystal structure of the EscN–EscO complex showed that EscO localises to the C-terminal opening of the hexameric EscN pore with the N- and C-terminal coiled-coil regions penetrating the pore (Majewski et al.,

2019). The finding that EscO can partially rescue the motility of a *fliJ* mutant supports the notion that both proteins share a similar function (Romo-Castillo et al., 2014).

It remains to be investigated whether also HrpB7 from Xcv contributes to the assembly of the ATPase complex and to the regulation of its activity as was reported for FliJ and EscO (Ibuki et al., 2011; Majewski et al., 2019). In preliminary in vitro experiments, however, we did not detect a positive influence of HrpB7 on the activity of the purified ATPase HrcN (J. Hausner and D. Büttner, unpublished data). Furthermore, our fluorescence microscopy studies showed that the predicted C ring component HrcQ assembles independently of HrpB7 (Figure 7). Given that a failure in the assembly of the ATPase complex likely results in a loss of C ring formation as shown in *Yersinia* spp. (Diepold et al., 2010), it is possible that HrpB7 is dispensable for the formation of the ATPase complex. Notably, a similar finding was reported for the HrpO/FliJ/YscO family member YscO from *Yersinia* spp., suggesting that a role in the assembly of the ATPase does not appear to be a general characteristic function of this protein family (Diepold et al., 2012).

HrpB7 does not only interact with components of the T3SS but also with the T3S chaperone HpaB as revealed by our interaction studies (Figure 7). Notably, an interaction with T3S chaperones was also described for FliJ, Spa13, and InvI, suggesting that HrpO/FliJ/YscO family members are involved in a network of interactions with T3SS components and chaperones (Evans et al., 2006; Evans & Hughes, 2009). In *Xcv*, the T3S chaperone HpaB is essential for the efficient secretion and translocation of multiple effector proteins and was previously identified as interaction partner of T3SS components including the ATPase, the C ring, and the cytoplasmic domains of components of the export apparatus (Büttner et al., 2004; Büttner et al., 2006; Hartmann & Büttner, 2013; Lonjon et al., 2017; Lorenz & Büttner, 2009; Lorenz et al., 2012; Prochaska et al., 2018). The presence of multiple binding sites for HpaB in the T3SS suggests that HrpB7 does not play an exclusive role in the recruitment of chaperone complexes but might rather be of general importance for T3S. This hypothesis is supported by the finding that HrpB7 is not only essential for the delivery of HpaB-dependent effector proteins but also for the translocation of the HpaB-independent early T3S substrate HrpB2 (Figure 3).

Given the variety of different interaction partners identified for HrpO/FliJ/YscO family members, it seems likely that the observed protein–protein interactions are stabilised by the coiled-coil motifs. We, therefore, analysed the predicted contribution of the putative coiled-coil motifs in HrpB7 to protein–protein interactions and protein function. Characteristic features of coiled coils are repetitive heptad motifs (abcdefg)$_n$ with hydrophobic amino acids at positions "a" and "d" (Gazi et al., 2009). The presence of unbranched amino acids such as leucine at position "a" as is the case in HrpB7 (Figure 1) might favour the formation of four-stranded parallel coiled coils (Lupas & Gruber, 2005). When we exchanged the leucine residues in the heptad motifs of HrpB7 against glycine, complex formation was severely impaired (Figure 6). Glycine is a known helix breaker and, therefore, likely affects the helical structures within the predicted coiled coils

(Serrano et al., 1992). HrpB7 derivatives with leucine-to-glycine exchanges in both predicted coiled-coil regions did not complement the *hrpB7* mutant phenotype and only weakly interacted with HrcQ, HrcD, and HpaB, suggesting an important role of these amino acids in HrpB7 function and protein–protein interactions (Figures 6 and 7). The exchange of leucine residues in N- and C-terminal heptad motifs against the polar amino acid serine also abolished detectable complex formation (Figure 6). However, HrpB7 derivatives with leucine-to-serine exchanges were partially functional, indicating that complex formation contributes to but is presumably not crucial for HrpB7 function. The observed negative impact of the mutations was strongly reduced when amino acid exchanges were only introduced in either the N- or the C-terminal heptad motif (Figure 6).

We also investigated the role of the five regularly spaced cysteine residues at position "d" of each N-terminal heptad in HrpB7. The exchange of all five cysteine residues in the N-terminal (C-$X_6)_5$ motif against alanine significantly reduced complex formation by HrpB7 (Figure 6). This is in agreement with the hypothesis that cysteine residues stabilise the coiled-coil structure by the formation of disulfide bonds and thus presumably contribute to the assembly of intermolecular or intramolecular complexes (Shen et al., 2005; Zhou et al., 1993). Given that alanine still fits the criteria for position "d" of the leucine heptad motif, the C-to-A exchange likely did not completely prevent coiled-coil formation. In line with this hypothesis is our finding that the C-to-A mutations impaired but did not abolish HrpB7 function (Figure 6). We conclude that HrpB7 function and complex formation depend on the leucine and cysteine residues in the N- and C-terminal heptad motifs but that single amino acids can be mutated without causing significant detrimental effects. This is in line with the finding that some of the cysteine and leucine residues in the N- and C-terminal heptad motifs are not conserved in HrpB7$_{Xcc}$, which is functional in *Xcv*.

Taken together, our study provides the first detailed characterisation of a member of the FliJ/HrpO/YscO family from a Hrp2-T3SS. The experimental results suggest that HrpB7 from *Xcv* forms an essential oligomeric structure of the T3SS and interacts via coiled coils with the ATPase complex as well as with IM and cytoplasmic rings of the T3SS. In future experiments, we will investigate whether HrpB7 contributes to the assembly of the ATPase complex or additional substructures of the T3SS.

4 | EXPERIMENTAL PROCEDURES

4.1 | Bacterial strains and growth conditions

Bacterial strains and plasmids are listed in Table S1. *E. coli* strains were cultivated at 37°C in lysogeny broth medium. *Xcv* strains were grown at 30°C in nutrient yeast extract glycerol medium (Daniels et al., 1984). For T3S assays, we used minimal medium A (MA) supplemented with sucrose (10 mM) and casamino acids (0.3%; Ausubel et al., 1996).

4.2 | Plant material and plant infections

For infection studies, bacterial solutions were infiltrated into leaves of the near-isogenic pepper cultivars ECW and ECW-10R with a needle-less syringe (Kousik & Ritchie, 1998; Minsavage et al., 1990). Plants were inoculated with 1×10^8 colony-forming units (CFU) ml^{-1} in 1-mM MgCl$_2$ if not stated otherwise. Infected plants were incubated in growth chambers for 16 hr of light at 28°C and 8 hr of darkness at 22°C. Plant reactions were monitored 1–9 days post inoculation (dpi). The HR was documented after destaining the leaves in 70% ethanol. Infection experiments were performed at least three times with different transconjugants; representative results are shown. *In planta* growth curves were performed three times as described (Bonas et al., 1991). To monitor translocation of dTALE-2, we used *gfp*-transgenic *N. benthamiana* plants (Werner et al., 2011). Infected *N. benthamiana* plants were incubated for 16 hr of light at 20°C and 8 hr of darkness at 18°C. GFP fluorescence was documented 4 dpi.

4.3 | Generation of Xcv hrpB7 deletion mutant strains

To generate *Xcv hrpB7* deletion mutants, DNA fragments flanking *hrpB7* and including the first and last 18 nucleotides of the coding sequence were amplified by polymerase chain reaction (PCR) and cloned into the Golden Gate-compatible suicide vector pOGG2 using BsaI and ligase. The resulting construct was transformed into *E. coli* DH5λpir and transferred into strains 85–10 and 85* by triparental conjugation. Transconjugants were selected as described previously (Huguet, et al., 1998). Double crossovers resulted in *hrpB7* deletion mutant strains.

4.4 | Generation of expression constructs

To generate a *hrpB7* expression construct, *hrpB7* was amplified by PCR from *Xcv* strain 85–10 and cloned into the BsaI sites of vector pBRM, downstream of a *lac* promoter and in frame with a C-terminal 3 × c-Myc epitope-encoding sequence. Similarly, *hrpB7* was cloned into vector pBRM-Stop, which contains a stop codon upstream of the 3 × c-Myc epitope-encoding sequence, resulting in the synthesis of untagged HrpB7. We also generated a pBRM expression construct encoding HrpB7 from *Xcv* using primers specific for *hrpB7*$_{Xcc}$ from strain LMG 568. For the generation of a GST-HrpB7 expression construct, two modules corresponding to *hrpB7* and *ptac-gst* were cloned into vector pBRM-P, resulting in construct pB-P-ptacGST-hrpB7. *ptac-gst* was amplified by PCR from vector pGEX-2TKM. All PCR amplicons were first subcloned into vector pUC57ΔBsaI or alternatively into vector pICH41021 using SmaI and ligase.

For the exchange of cysteine residues against alanine, 5′ and 3′ regions of *hrpB7* were amplified by PCR from plasmid pBhrpB7*, in

which the internal BsaI site in *hrpB7* had been mutated by PCR. Mutations leading to exchanges of cysteine residues at positions 29, 36, 43, 50, 57, and 90 against alanine were introduced by the primer sequences. Cloning of PCR products into the BsaI sites of vectors pBRM and pBRM-Stop led to the generation of expression constructs encoding HrpB7$_{C43A}$ (HrpB7$_{C3A}$), HrpB7$_{C29,36A}$ (HrpB7$_{C1-2A}$), HrpB7$_{C29,36,43A}$ (HrpB7$_{C1-3A}$), HrpB7$_{C29,36,43,50,57A}$ (HrpB7$_{C1-5A}$), HrpB7$_{C90A}$ (HrpB7$_{C6A}$), and HrpB7$_{C29,36,43,50,57,90A}$ (HrpB7$_{C1-6A}$) with or without C-terminal c-Myc epitope. Primers used for the generation of HrpB7$_{C43A}$ (HrpB7$_{C3A}$) were designed to introduce three mutations but only resulted in the C43A mutation. *hrpB7$_{C3A}$* was, therefore, used as PCR template to generate a *hrpB7$_{C1-3A}$* expression construct. Similarly, *hrpB7$_{C1-3A}$* was used as template to generate a *hrpB7$_{C1-5A}$* expression construct, which was subsequently used as a template to generate *hrpB7$_{C1-6A}$*.

For the generation of expression constructs encoding HrpB7 derivatives with exchanged leucine residues, the corresponding mutations were introduced by PCR. For each mutant derivative, the 5′ and 3′ regions of *hrpB7* were amplified by PCR, and the mutations were introduced by the primer sequences. PCR products were cloned into vectors pBRM and pBRM-Stop, resulting in expression constructs for the synthesis of HrpB7 derivatives with mutations in the N- or C-terminal or in both leucine heptad motifs, which were referred to as L1S (HrpB7$_{L33,40S}$), L1G (HrpB7$_{L33,40G}$), L2S (HrpB7$_{L111,118S}$), L2G (HrpB7$_{L111,118G}$), L12S (HrpB7$_{L33,40,111,118S}$), and L12G (HrpB7$_{L33,40,111,118G}$). *hrpB7$_{L12G}$* was amplified by PCR from pBStophrpB7$_{L12G}$ and cloned together with *ptac-gst* into vector pBRM-P, thus generating an expression construct that encodes GST-HrpB7$_{L12G}$. In addition to the generation of *hrpB7* expression constructs, we amplified *hrcD* and cloned the corresponding PCR product in vector pBRM. Generated constructs and primers used in this study are listed in Tables S1 and S2, respectively.

For the construction of PhoA$_{\Delta2-120}$ expression constructs, the *phoA$_{\Delta2-120}$* gene fragment from *E. coli* (GenBank accession number M29668) including an additional linker-encoding sequence (amino acids LSLIHISWPMGPG) was amplified using nested forward primers containing the linker-encoding sequence and a *phoA*-specific reverse primer (see Table S1; Berger et al., 2010). The linker-*phoA$_{\Delta2-120}$* gene fragment was subcloned into vector pICH41021 using SmaI and ligase and subsequently ligated with *hrpB7* into vector pBRM, resulting in pBhrpB7-linker-phoA$_{\Delta2-120}$. To generate constructs encoding PhoA$_{\Delta2-120}$ as N-terminal fusion partner of HrpB7, the linker-*phoA$_{\Delta2-120}$* gene fragment was amplified from construct pICH41021-linker-*phoA$_{\Delta2-120}$* using primers that allow cloning of the linker-*phoA$_{\Delta2-120}$* fragment into the 5′ cloning site (5′-TATG-3′ overhang) of vector pBRM. Ligation of linker-*phoA$_{\Delta2-120}$* with *hrpB7* into vector pBRM using BsaI and ligase resulted in an expression construct encoding Linker-PhoA$_{\Delta2-120}$-HrpB7. PhoA$_{\Delta2-120}$ expression constructs were transferred into strain 85*Δ*hrpB7* for complementation studies and into strain 85*Δ*phoA* for the analysis of the phosphatase activity. PhoA$_{\Delta2-120}$ fusion proteins were detected by immunoblotting using a PhoA-specific antibody (Sigma-Aldrich).

4.5 | Generation of a modular T3S gene cluster construct containing *hrcQ-sfgfp* and deletions in *hrcQ* and *hrpB7*

To introduce a deletion into *hrpB7* in the modular T3S gene cluster, *hrpB7* was amplified by PCR with primers FShrpB7_F and FShrpB7_R using the level −2 construct pAGB194, which contains *hrpB7*, as template (Hausner et al., 2019). The resulting PCR amplicon corresponding to *hrpB7* with a deletion of bp 15 to 429 was cloned into the pUC19 derivative pAGM9121 (Addgene #51833) using BpiI and ligase, thus generating the level −2 construct pAGB772. In a subsequent Golden Gate reaction, the insert of pAGB772 was assembled with modules from additional level −2 constructs pAGB192 (contains *hrcL*), pAGB193 (contains *hrcN*), pAGB195 (contains *hrcT*), and pAGB196 (contains *hrcC*) in Level −1 vector pAGM1311 (Addgene #47983) using BsaI and ligase (Hausner et al., 2019). The assembly of the resulting pAGB778 construct with the additional level −1 construct pAGB197, which contains *hrpB1* to *hrpB4*, using BpiI and ligase led to Level 0 construct pAGB784 (corresponding to the *hrpA* and *hrpB* operons), which was subsequently cloned into level 1 vector pICH47811 using BsaI and ligase (Addgene #48008), thus generating level 1 construct pAGB790. The assembly by BpiI and ligase with additional level 1 constructs pAGB275 (contains *hrpC–hpaB* operons with a deletion in *hrcQ*) and pAGB156 (contains *hrpF*) led to the generation of level M construct pAGB796, which includes the *hrp* gene cluster with deletions in *hrpB7* and *hrcQ* (Hausner et al., 2019). Construct pAGB796 was assembled with level M construct pAGB322 (contains *xopA*, *hpaH*, *hrpX*, *hrpG**, and *hrcQ-sfgfp*; Hausner et al., 2019) and end-linker pICH79264 in level P vector pICH75322 using BsaI and ligase, thus resulting in the final level P construct pAGB802.

4.6 | Analysis of in vitro T3S

In vitro T3S assays were performed as described previously (Rossier et al., 1999). Briefly, bacteria were grown overnight in MA medium (pH 7.0) supplemented with sucrose (10 mM) and casamino acids (0.3%) and shifted to MA medium (pH 5.3) containing 50-μg ml^{-1} bovine serum albumin (BSA) and 10-μM thiamine at an optical density (OD$_{600\ nm}$) of 0.15. Cultures were incubated on a rotary shaker for 1.5 hr at 30°C, and bacterial cells and secreted proteins were separated by filtration. Proteins in 2 ml of the culture supernatants were precipitated with trichloroacetic acid and resuspended in 20 μl of Laemmli buffer. Total cell extracts and culture supernatants were analysed by SDS-PAGE and immunoblotting, using antibodies directed against the c-Myc epitope as well as against HrpB7, HrpF, HrcJ, and AvrBs3, respectively (Bonas et al., unpublished; Büttner et al., 2002; Knoop et al., 1991; Rossier et al., 2000). Horseradish peroxidase-labelled anti-mouse and anti-goat antibodies were used as secondary antibodies, and binding of antibodies was visualised by enhanced chemiluminescence.

4.7 | GST pull-down assays

For GST pull-down assays, *E. coli* BL21(DE3) cells containing the expression constructs for the synthesis of GST, GST-HrpB7, GST-HrpB7$_{L12G}$, and C-terminally c-Myc epitope-tagged potential interaction partners were grown in lysogeny broth medium until an OD$_{600\ nm}$ of 0.6–0.8. Gene expression, which was driven in all cases by the *lac* promoter, was induced in the presence of IPTG for 2 hr at 37°C, and after centrifugation bacterial cells were broken with a French press. Cell debris was removed by centrifugation, and soluble GST and GST fusion proteins were immobilised on a glutathione sepharose matrix according to the manufacturer's instructions (GE Healthcare). After washing of the matrix, immobilised GST and GST-HrpB7 were incubated with bacterial lysates containing the predicted interaction partner for 2 hr at 4°C on an overhead shaker. Unbound proteins were removed by washing, and bound proteins were eluted with Laemmli buffer. Cell lysates and eluted proteins were analysed by SDS-PAGE and immunoblotting, using c-Myc epitope- and GST-specific antibodies.

4.8 | Fractionation experiments with *Xcv* strains

For the subcellular localisation of HrpB7, bacteria were grown overnight in MA medium (pH 7.0) supplemented with sucrose (10 mM) and casamino acids (0.3%). Bacteria from the overnight culture were used to inoculate 50-ml MA (pH 5.3) medium supplemented with sucrose (10 mM), casamino acids (0.3%), 50-μg/ml BSA, and 10-μM thiamine at on OD$_{600\ nm}$ of 0.1. The culture was incubated overnight on a shaker. Cells were then harvested by centrifugation, resuspended in 2-ml 50 mM HEPES (2-(4-[2-hydroxyethyl]-1-piperazinylethanesulfonic acid) and lysed with a French press. Cell debris was removed by centrifugation and lysates were centrifuged at 200.000 × g for 90 min at 4°C. The pellet corresponding to the membrane fraction was resuspended in 1-ml 50 mM HEPES buffer. Samples of membrane and soluble fractions were mixed with Laemmli buffer and analysed by immunoblotting using c-Myc epitope- and HrcJ-specific antibodies. For the analysis of membrane-associated proteins, the pellet after ultracentrifugation was resuspended in 1-ml 50-mM HEPES buffer in the presence of 5-M urea and stirred for 1 hr at 4°C. The solution was centrifuged at 200.000 × g for 90 min at 4°C. Samples of the supernatants and the pellets corresponding to the membrane-associated and the integral membrane proteins, respectively, were mixed with Laemmli buffer and analysed by immunoblotting as described above.

4.9 | Phosphatase assays

For the analysis of the PhoA activity, bacteria were resuspended in secretion medium at an OD$_{600nm}$ of 0.8 and incubated in the presence of 90-μg/ml X-Phos (5-Bromo-4-chloro-3-indolyl phosphate) on a horizontal shaker for 3 hr at 30°C. The colour change was photographed, and bacterial cell extracts were analysed by immunoblotting using a PhoA-specific antibody (Sigma-Aldrich). The phosphatase assay was performed twice with similar results.

4.10 | Fluorescence microscopy

For the analysis of HrcQ-sfGFP, bacteria were grown overnight in MA medium (pH 7.0) supplemented with sucrose (10 mM) and casamino acids (0.3%). Cells were then resuspended at an OD$_{600\ nm}$ of 0.15 in MA medium (pH 5.3) supplemented with BSA and thiamine as described above and incubated on a tube rotator at 30°C for 1 hr. Cell suspensions were pipetted on a microscopy slide on top of a pad of 1% agarose dissolved in MA medium (pH 5.3) containing BSA and thiamine as described previously (Hausner et al., 2019). GFP fluorescence was inspected with a confocal laser scanning microscope (Zeiss LSM 780 AxioObserver. Z1) using filter sets for sfGFP (excitation at 485 nm; emission at 510 nm). Experiments were performed with different transconjugants for each strain and repeated twice with similar results.

ORCID

Daniela Büttner https://orcid.org/0000-0003-3702-4172

REFERENCES

Abby, S. S., & Rocha, E. P. (2012). The non-flagellar type III secretion system evolved from the bacterial flagellum and diversified into host-cell adapted systems. *PLoS Genetics*, *8*, e1002983.

Alfano, J. R., & Collmer, A. (1997). The type III (Hrp) secretion pathway of plant pathogenic bacteria: Trafficking harpins, Avr proteins, and death. *Journal of Bacteriology*, *179*, 5655–5662.

Ausubel, F. M., Brent, R., Kingston, R. E., Moore, D. D., Seidman, J. G., Smith, J. A., & Struhl, K. (1996). *Current protocols in molecular biology*. In New York: John Wiley & Sons, Inc.

Berger, C., Robin, G. P., Bonas, U., & Koebnik, R. (2010). Membrane topology of conserved components of the type III secretion system from the plant pathogen *Xanthomonas campestris* pv. *vesicatoria*. *Microbiology*, *156*, 1963–1974.

Boch, J., Scholze, H., Schornack, S., Landgraf, A., Hahn, S., Kay, S., … Bonas, U. (2009). Breaking the code of DNA-binding specificity of TAL-type III effectors. *Science*, *326*, 1509–1512.

Bogdanove, A., Beer, S. V., Bonas, U., Boucher, C. A., Collmer, A., Coplin, D. L., … Van Gijsegem, F. (1996). Unified nomenclature for broadly conserved *hrp* genes of phytopathogenic bacteria. *Molecular Microbiology*, *20*, 681–683.

Bonas, U., Schulte, R., Fenselau, S., Minsavage, G. V., Staskawicz, B. J., & Stall, R. E. (1991). Isolation of a gene-cluster from *Xanthomonas campestris* pv. *vesicatoria* that determines pathogenicity and the

hypersensitive response on pepper and tomato. *Molecular Plant Microbe Interaction*, *4*, 81–88.

Büttner, D. (2012). Protein export according to schedule – Architecture, assembly and regulation of type III secretion systems from plant and animal pathogenic bacteria. *Microbiology and Molecular Biology Reviews*, *76*, 262–310.

Büttner, D. (2016). Behind the lines — actions of bacterial type III effector proteins in plant cells. *FEMS Microbiology Reviews*, *40*, 894–937.

Büttner, D., & Bonas, U. (2002). Getting across-bacterial type III effector proteins on their way to the plant cell. *EMBO Journal*, *21*, 5313–5322.

Büttner, D., & Bonas, U. (2010). Regulation and secretion of *Xanthomonas* virulence factors. *FEMS Microbiology Reviews*, *34*, 107–133.

Büttner, D., Gürlebeck, D., Noël, L. D., & Bonas, U. (2004). HpaB from *Xanthomonas campestris* pv. *vesicatoria* acts as an exit control protein in type III-dependent protein secretion. *Molecular Microbiology*, *54*, 755–768.

Büttner, D., & He, S. Y. (2009). Type III protein secretion in plant pathogenic bacteria. *Plant Physiology*, *150*, 1656–1664.

Büttner, D., Lorenz, C., Weber, E., & Bonas, U. (2006). Targeting of two effector protein classes to the Type III secretion system by a HpaC- and HpaB-dependent protein complex from *Xanthomonas campestris* pv. *vesicatoria*. *Molecular Microbiology*, *59*, 513–527.

Büttner, D., Nennstiel, D., Klüsener, B., & Bonas, U. (2002). Functional analysis of HrpF, a putative type III translocon protein from *Xanthomonas campestris* pv. Vesicatoria. *Journal of Bacteriology*, *184*, 2389–2398.

Cherradi, Y., Hachani, A., & Allaoui, A. (2014). Spa13 of *Shigella flexneri* has a dual role: Chaperone escort and export gate-activator switch of the type III secretion system. *Microbiology*, *160*, 130–141.

Daniels, M. J., Barber, C. E., Turner, P. C., Cleary, W. G., & Sawczyc, M. K. (1984). Isolation of mutants of *Xanthomonas campestris* pathovar *campestris* showing altered pathogenicity. *Journal of General Microbiology*, *130*, 2447–2455.

Dean, P. (2011). Functional domains and motifs of bacterial Type III effector proteins and their roles in infection. *FEMS Microbiology Reviews*, *35*, 1100–1125.

Delahay, R. M., & Frankel, G. (2002). Coiled-coil proteins associated with type III secretion systems: A versatile domain revisited. *Molecular Microbiology*, *45*, 905–916.

Deng, W., Marshall, N. C., Rowland, J. L., McCoy, J. M., Worrall, L. J., Santos, A. S., … Finlay, B. B. (2017). Assembly, structure, function and regulation of type III secretion systems. *Nature Reviews Microbiology*, *15*, 323–337.

Diepold, A., Amstutz, M., Abel, S., Sorg, I., Jenal, U., & Cornelis, G. R. (2010). Deciphering the assembly of the *Yersinia* type III secretion injectisome. *EMBO Journal*, *29*, 1928–1940.

Diepold, A., Kudryashev, M., Delalez, N. J., Berry, R. M., & Armitage, J. P. (2015). Composition, formation, and regulation of the cytosolic c-ring, a dynamic component of the type III secretion injectisome. *PLoS Biology*, *13*, e1002039.

Diepold, A., & Wagner, S. (2014). Assembly of the bacterial type III secretion machinery. *FEMS Microbiology Reviews*, *38*, 802–822.

Diepold, A., Wiesand, U., Amstutz, M., & Cornelis, G. R. (2012). Assembly of the *Yersinia* injectisome: The missing pieces. *Molecular Microbiology*, *85*, 878–892.

Diepold, A., Wiesand, U., & Cornelis, G. R. (2011). The assembly of the export apparatus (YscR,S,T,U,V) of the *Yersinia* type III secretion apparatus occurs independently of other structural components and involves the formation of an YscV oligomer. *Molecular Microbiology*, *82*, 502–514.

Evans, L. D., & Hughes, C. (2009). Selective binding of virulence type III export chaperones by FliJ escort orthologues InvI and YscO. *FEMS Microbiology Letters*, *293*, 292–297.

Evans, L. D., Stafford, G. P., Ahmed, S., Fraser, G. M., & Hughes, C. (2006). An escort mechanism for cycling of export chaperones during flagellum assembly. *Proceedings of the National Academy of Sciences USA*, *103*, 17474–17479.

Fenselau, S., & Bonas, U. (1995). Sequence and expression analysis of the *hrpB* pathogenicity operon of *Xanthomonas campestris* pv. *vesicatoria* which encodes eight proteins with similarity to components of the Hrp, Ysc, Spa, and Fli secretion systems. *Molecular Plant-Microbe Interactions*, *8*, 845–854.

Fraser, G. M., Gonzalez-Pedrajo, B., Tame, J. R., & Macnab, R. M. (2003). Interactions of FliJ with the *Salmonella* type III flagellar export apparatus. *Journal of Bacteriology*, *185*, 5546–5554.

Gazi, A. D., Bastaki, M., Charova, S. N., Gkougkoulia, E. A., Kapellios, E. A., Panopoulos, N. J., & Kokkinidis, M. (2008). Evidence for a coiled-coil interaction mode of disordered proteins from bacterial type III secretion systems. *Journal of Biological Chemistry*, *283*, 34062–34068.

Gazi, A. D., Charova, S. N., Panopoulos, N. J., & Kokkinidis, M. (2009). Coiled-coils in type III secretion systems: Structural flexibility, disorder and biological implications. *Cellular Microbiology*, *11*, 719–729.

Gill, U. S., Lee, S., & Mysore, K. S. (2015). Host versus nonhost resistance: Distinct wars with similar arsenals. *Phytopathology*, *105*, 580–587.

Hartmann, N., & Büttner, D. (2013). The inner membrane protein HrcV from *Xanthomonas* is involved in substrate docking during type III secretion. *Molecular Plant-Microbe Interactions*, *26*, 1176–1189.

Hartmann, N., Schulz, S., Lorenz, C., Fraas, S., Hause, G., & Büttner, D. (2012). Characterization of HrpB2 from *Xanthomonas campestris* pv. *vesicatoria* identifies protein regions that are essential for type III secretion pilus formation. *Microbiology*, *158*, 1334–1349.

Hausner, J., Hartmann, N., Jordan, M., & Büttner, D. (2017). The predicted lytic transglycosylase HpaH from *Xanthomonas campestris* pv. *vesicatoria* associates with the type III secretion system and promotes effector protein translocation. *Infection and Immunity*, *85*, e00788–e00716.

Hausner, J., Hartmann, N., Lorenz, C., & Büttner, D. (2013). The periplasmic HrpB1 protein from *Xanthomonas* spp. binds to peptidoglycan and to components of the type III secretion system. *Applied and Environmental Microbiology*, *79*, 6312–6324.

Hausner, J., Jordan, M., Otten, C., Marillonnet, S., & Büttner, D. (2019). Modular cloning of the type III secretion gene cluster from the plant-pathogenic bacterium *Xanthomonas euvesicatoria*. *ACS Synthetic Biology*, *8*, 532–547.

Hu, B., Morado, D. R., Margolin, W., Rohde, J. R., Arizmendi, O., Picking, W. L., … Liu, J. (2015). Visualization of the type III secretion sorting platform of *Shigella flexneri*. *Proceedings of the National Academy of Sciences USA*, *112*, 1047–1052.

Hueck, C. J. (1998). Type III protein secretion systems in bacterial pathogens of animals and plants. *Microbiology and Molecular Biology Reviews*, *62*, 379–433.

Huguet, E., Hahn, K., Wengelnik, K., & Bonas, U. (1998). *hpaA* mutants of *Xanthomonas campestris* pv. *vesicatoria* are affected in pathogenicity but retain the ability to induce host-specific hypersensitive reaction. *Molecular Microbiology*, *29*, 1379–1390.

Ibuki, T., Imada, K., Minamino, T., Kato, T., Miyata, T., & Namba, K. (2011). Common architecture of the flagellar type III protein export apparatus and F- and V-type ATPases. *Nature Structural & Molecular Biology*, *18*, 277–282.

Jones, J. B., Lacy, G. H., Bouzar, H., Stall, R. E., & Schaad, N. W. (2004). Reclassification of the xanthomonads associated with bacterial spot disease of tomato and pepper. *Systematic and Applied Microbiology*, *27*, 755–762.

Kelley, L. A., Mezulis, S., Yates, C. M., Wass, M. N., & Sternberg, M. J. (2015). The Phyre2 web portal for protein modeling, prediction and analysis. *Nature Protocols*, *10*, 845–858.

Knoop, V., Staskawicz, B., & Bonas, U. (1991). Expression of the avirulence gene *avrBs3* from *Xanthomonas campestris* pv. *vesicatoria* is not under the control of *hrp* genes and is independent of plant factors. *Journal of Bacteriology*, *173*, 7142–7150.

Koebnik, R., Krüger, A., Thieme, F., Urban, A., & Bonas, U. (2006). Specific binding of the *Xanthomonas campestris* pv. *vesicatoria* AraC-type transcriptional activator HrpX to plant-inducible promoter boxes. *Journal of Bacteriology*, 188, 7652–7660.

Kousik, C. S., & Ritchie, D. F. (1998). Response of bell pepper cultivars to bacterial spot pathogen races that individually overcome major resistance genes. *Plant Disease*, 82, 181–186.

Lara-Tejero, M. (2019). *The type III secretion system sorting platform. Current topics in microbiology and immunology*. Berlin, Heidelberg: Springer.

Lara-Tejero, M., & Galan, J. E. (2019). The injectisome, a complex nanomachine for protein injection into mammalian cells. *EcoSal Plus*, 8.

Li, H., & Sourjik, V. (2011). Assembly and stability of flagellar motor in *Escherichia coli*. *Molecular Microbiology*, 80, 886–899.

Li, Y. R., Zou, H. S., Che, Y. Z., Cui, Y. P., Guo, W., Zou, L. F., ... Chen, G. Y. (2011). A novel regulatory role of HrpD6 in regulating *hrp-hrc-hpa* genes in *Xanthomonas oryzica* pv. *oryzicola*. *Molecular Plant-Microbe Interactions*, 24, 1086–1101.

Liu, Z. Y., Zou, L. F., Xue, X. B., Cai, L. L., Ma, W. X., Xiong, L., ... Chen, G. Y. (2014). HrcT is a key component of the type III secretion system in *Xanthomonas* and also regulates the expression of the key *hrp* transcriptional activator HrpX. *Applied and Environmental Microbiology*, 80, 3908–3919.

Lonjon, F., Lohou, D., Cazale, A. C., Büttner, D., Ribeiro, B. G., Peanne, C., ... Vailleau, F. (2017). HpaB-Dependent secretion of type III effectors in the plant pathogens *Ralstonia solanacearum* and *Xanthomonas campestris* pv. *vesicatoria*. *Scientific Reports*, 7, 4879.

Lorenz, C., & Büttner, D. (2009). Functional characterization of the type III secretion ATPase HrcN from the plant pathogen *Xanthomonas campestris* pv. *vesicatoria*. *Journal of Bacteriology*, 191, 1414–1428.

Lorenz, C., & Büttner, D. (2011). Secretion of early and late substrates of the type III secretion system from *Xanthomonas* is controlled by HpaC and the C-terminal domain of HrcU. *Molecular Microbiology*, 79, 447–467.

Lorenz, C., Hausner, J., & Büttner, D. (2012). HrcQ provides a docking site for early and late type III secretion substrates from *Xanthomonas*. *PLoS One*, 7, e51063.

Lupas, A. N., & Gruber, M. (2005). The structure of alpha-helical coiled coils. *Advances in Protein Chemistry*, 70, 37–78.

Majewski, D. D., Worrall, L. J., Hong, C., Atkinson, C. E., Vuckovic, M., Watanabe, N., ... Strynadka, N. C. J. (2019). Cryo-EM structure of the homohexameric T3SS ATPase-central stalk complex reveals rotary ATPase-like asymmetry. *Nature Communications*, 10, 626.

Makino, F., Shen, D., Kajimura, N., Kawamoto, A., Pissaridou, P., Oswin, H., ... Blocker, A. J. (2016). The architecture of the cytoplasmic region of type III secretion systems. *Scientific Reports*, 6, 33341.

Manoil, C., & Beckwith, J. (1986). A genetic approach to analyzing membrane protein topology. *Science*, 233, 1403–1408.

Mason, J. M., & Arndt, K. M. (2004). Coiled coil domains: Stability, specificity, and biological implications. *Chembiochem*, 5, 170–176.

Minsavage, G. V., Dahlbeck, D., Whalen, M. C., Kearny, B., Bonas, U., Staskawicz, B. J., & Stall, R. E. (1990). Gene-for-gene relationships specifying disease resistance in *Xanthomonas campestris* pv. *vesicatoria* - pepper interactions. *Molecular Plant-Microbe Interactions*, 3, 41–47.

Morimoto, Y. V., Ito, M., Hiraoka, K. D., Che, Y. S., Bai, F., Kami-Ike, N., ... Minamino, T. (2014). Assembly and stoichiometry of FliF and FlhA in *Salmonella* flagellar basal body. *Molecular Microbiology*, 91, 1214–1226.

Morita-Ishihara, T., Ogawa, M., Sagara, H., Yoshida, M., Katayama, E., & Sasakawa, C. (2006). *Shigella* Spa33 is an essential C-ring component of type III secretion machinery. *Journal of Biological Chemistry*, 281, 599–607.

Noël, L., Thieme, F., Gäbler, J., Büttner, D., & Bonas, U. (2003). XopC and XopJ, two novel type III effector proteins from *Xanthomonas campestris* pv. *vesicatoria*. *Journal of Bacteriology*, 185, 7092–7102.

Noël, L., Thieme, F., Nennstiel, D., & Bonas, U. (2001). cDNA-AFLP analysis unravels a genome-wide *hrpG*-regulon in the plant pathogen *Xanthomonas campestris* pv. *vesicatoria*. *Molecular Microbiology*, 41, 1271–1281.

Prochaska, H., Thieme, S., Daum, S., Grau, J., Schmidtke, C., Hallensleben, M., ... Bonas, U. (2018). A conserved motif promotes HpaB-regulated export of type III effectors from *Xanthomonas*. *Molecular Plant Pathology*, 19, 2473–2487.

Römer, P., Strauss, T., Hahn, S., Scholze, H., Morbitzer, R., Grau, J., ... Lahaye, T. (2009). Recognition of AvrBs3-like proteins is mediated by specific binding to promoters of matching pepper *Bs3* alleles. *Plant Physiology*, 150, 1697–1712.

Romo-Castillo, M., Andrade, A., Espinosa, N., Monjaras Feria, J., Soto, E., Diaz-Guerrero, M., & Gonzalez-Pedrajo, B. (2014). EscO, a functional and structural analog of the flagellar FliJ protein, is a positive regulator of EscN ATPase activity of the enteropathogenic *Escherichia coli* injectisome. *Journal of Bacteriology*, 196, 2227–2241.

Rossier, O., Van den Ackerveken, G., & Bonas, U. (2000). HrpB2 and HrpF from *Xanthomonas* are type III-secreted proteins and essential for pathogenicity and recognition by the host plant. *Molecular Microbiology*, 38, 828–838.

Rossier, O., Wengelnik, K., Hahn, K., & Bonas, U. (1999). The *Xanthomonas* Hrp type III system secretes proteins from plant and mammalian pathogens. *Proceedings of the National Academy of Sciences USA*, 96, 9368–9373.

Scheibner, F., Hartmann, N., Hausner, J., Lorenz, C., Hoffmeister, A. K., & Büttner, D. (2018). The type III secretion chaperone HpaB controls the translocation of effector and non-effector proteins from *Xanthomonas campestris* pv. *vesicatoria*. *Molecular Plant-Microbe Interactions*, 31, 61–74.

Scheibner, F., Schulz, S., Hausner, J., Marillonnet, S., & Büttner, D. (2016). Type III-dependent translocation of HrpB2 by a non-pathogenic *hpaABC* mutant of the plant-pathogenic bacterium *Xanthomonas campestris* pv. *vesicatoria*. *Applied and Environmental Microbiology*, 82, 3331–3347.

Schmidt, H., & Hensel, M. (2004). Pathogenicity islands in bacterial pathogenesis. *Clinical Microbiology Reviews*, 17, 14–56.

Serrano, L., Neira, J. L., Sancho, J., & Fersht, A. R. (1992). Effect of alanine versus glycine in alpha-helices on protein stability. *Nature*, 356, 453–455.

Shen, W., Lammertink, R. G. H., Sakata, J. K., Kornfield, J. A., & Tirrell, D. A. (2005). Assembly of an artificial protein hydrogel through leucine zipper aggregation and disulfide bond formation. *Macromolecules*, 38, 3909–3916.

Spaeth, K. E., Chen, Y. S., & Valdivia, R. H. (2009). The *Chlamydia* type III secretion system C-ring engages a chaperone-effector protein complex. *PLoS Pathogens*, 5, e1000579.

Szurek, B., Rossier, O., Hause, G., & Bonas, U. (2002). Type III-dependent translocation of the *Xanthomonas* AvrBs3 protein into the plant cell. *Molecular Microbiology*, 46, 13–23.

Tampakaki, A. P., Skandalis, N., Gazi, A. D., Bastaki, M. N., Sarris, P. F., Charova, S. N., ... Panopoulos, N. J. (2010). Playing the "harp": Evolution of our understanding of hrp/hrc genes. *Annual Review of Phytopathology*, 48, 347–370.

Troisfontaines, P., & Cornelis, G. R. (2005). Type III secretion: More systems than you think. *Physiologia Plantarum*, 20, 326–339.

Uversky, V. N. (2013). Intrinsic disorder-based protein interactions and their modulators. *Current Pharma Design*, 19, 4191–4213.

Van Gijsegem, F., Vasse, J., De Rycke, R., Castello, P., & Boucher, C. (2002). Genetic dissection of *Ralstonia solanacearum* hrp gene cluster reveals that the HrpV and HrpX proteins are required for Hrp pilus assembly. *Molecular Microbiology*, 44, 935–946.

Waterhouse, A., Bertoni, M., Bienert, S., Studer, G., Tauriello, G., Gumienny, R., ... Schwede, T. (2018). SWISS-MODEL: Homology

modelling of protein structures and complexes. *Nucleic Acids Research*, *46*, W296–W303.

Weber, E., Gruetzner, R., Werner, S., Engler, C., & Marillonnet, S. (2011). Assembly of designer TAL effectors by Golden Gate cloning. *PLoS One*, *6*, e19722.

Weber, E., & Koebnik, R. (2005). Domain structure of HrpE, the Hrp pilus subunit of *Xanthomonas campestris* pv. *vesicatoria*. *Journal of Bacteriology*, *187*, 6175–6186.

Weber, E., Ojanen-Reuhs, T., Huguet, E., Hause, G., Romantschuk, M., Korhonen, T. K., … Koebnik, R. (2005). The type III-dependent Hrp pilus is required for productive interaction of *Xanthomonas campestris* pv. *vesicatoria* with pepper host plants. *Journal of Bacteriology*, *187*, 2458–2468.

Wengelnik, K., & Bonas, U. (1996). HrpXv, an AraC-type regulator, activates expression of five of the six loci in the *hrp* cluster of *Xanthomonas campestris* pv. *vesicatoria*. *Journal of Bacteriology*, *178*, 3462–3469.

Wengelnik, K., Rossier, O., & Bonas, U. (1999). Mutations in the regulatory gene *hrpG* of *Xanthomonas campestris* pv. *vesicatoria* result in constitutive expression of all *hrp* genes. *Journal of Bacteriology*, *181*, 6828–6831.

Wengelnik, K., Van den Ackerveken, G., & Bonas, U. (1996). HrpG, a key *hrp* regulatory protein of *Xanthomonas campestris* pv. *vesicatoria* is homologous to two-component response regulators. *Molecular Plant-Microbe Interactions*, *9*, 704–712.

Werner, S., Breus, O., Symonenko, Y., Marillonnet, S., & Gleba, Y. (2011). High-level recombinant protein expression in transgenic plants by using a double-inducible viral vector. *Proceedings of the National Academy of Sciences USA*, *108*, 14061–14066.

Woolfson, D. N., Bartlett, G. J., Bruning, M., & Thomson, A. R. (2012). New currency for old rope: From coiled-coil assemblies to alpha-helical barrels. *Current Opinion in Structural Biology*, *22*, 432–441.

Zhang, Y., Lara-Tejero, M., Bewersdorf, J., & Galan, J. E. (2017). Visualization and characterization of individual type III protein secretion machines in live bacteria. *Proceedings of the National Academy of Sciences USA*, *114*, 6098–6103.

Zhou, N. E., Kay, C. M., & Hodges, R. S. (1993). Disulfide bond contribution to protein stability: Positional effects of substitution in the hydrophobic core of the two-stranded alpha-helical coiled-coil. *Biochemistry*, *32*, 3178–3187.

SUPPORTING INFORMATION

Additional supporting information may be found online in the Supporting Information section at the end of this article.